https://doi.org/10.1093/plcell/koac133 THE PLANT CELL 2022: 34: 2969–2988

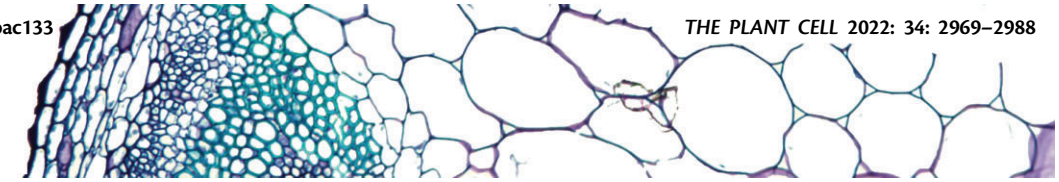

Research Article

A coiled-coil protein associates Polycomb Repressive Complex 2 with KNOX/BELL transcription factors to maintain silencing of cell differentiation-promoting genes in the shoot apex

Feng-Quan Tan ,[1] Wentao Wang ,[1] Junjie Li ,[1] Yue Lu ,[2] Bo Zhu ,[1] Fangfang Hu ,[1] Qi Li ,[1] Yu Zhao [1,*] and Dao-Xiu Zhou [1,3,*]

1 National Key Laboratory of Crop Genetic Improvement, Hubei Hongshan Laboratory, Huazhong Agricultural University, Wuhan 430070, China
2 Jiangsu Key Laboratory of Crop Genomics and Molecular Breeding/Key Laboratory of Plant Functional Genomics of the Ministry of Education, College of Agriculture, Yangzhou University, Yangzhou 225009, China
3 Institute of Plant Science Paris-Saclay (IPS2), CNRS, INRAE, University Paris-Saclay, Orsay 91405, France

*Authors for correspondence: zhaoyu@mail.hzau.edu.cn (Y.Z.); dao-xiu.zhou@universite-paris-saclay.fr (D.X.Z.)
These authors contributed equally (F-Q.T. and W.W.)
F.T. did the late phase of the work and W.W. did the early phase of the work. J.L., F.H., and Q.L. participated in the experiments. Y.L. and B.Z. did data analysis, Y.Z. and D.X.Z. designed and supervised the work. D.X.Z. wrote the paper with input from F.T., W.W., and Y.Z. We thank Qinglu Zhang for help with field experiments.
The author responsible for distribution of materials integral to the findings presented in this article in accordance with the policy described in the Instructions for Authors (https://academic.oup.com/plcell) is: Dao-Xiu Zhou (dao-xiu.zhou@universite-paris-saclay.fr).

Abstract

Polycomb repressive complex 2 (PRC2), which mediates the deposition of H3K27me3 histone marks, is important for developmental decisions in animals and plants. In the shoot apical meristem (SAM), Three Amino acid Loop Extension family *KNOTTED-LIKE HOMEOBOX* /BEL-like (KNOX/BELL) transcription factors are key regulators of meristem cell pluripotency and differentiation. Here, we identified a PRC2-associated coiled-coil protein (PACP) that interacts with KNOX/BELL transcription factors in rice (*Oryza sativa*) shoot apex cells. A loss-of-function mutation of *PACP* resulted in differential gene expression similar to that observed in PRC2 gene knockdown plants, reduced H3K27me3 levels, and reduced genome-wide binding of the PRC2 core component EMF2b. The genomic binding of PACP displayed a similar distribution pattern to EMF2b, and genomic regions with high PACP- and EMF2b-binding signals were marked by high levels of H3K27me3. We show that PACP is required for the repression of cell differentiation-promoting genes targeted by a rice KNOX1 protein in the SAM. PACP is involved in the recruitment or stabilization of PRC2 to genes targeted by KNOX/BELL transcription factors to maintain H3K27me3 and gene repression in dividing cells of the shoot apex. Our results provide insight into PRC2-mediated maintenance of H3K27me3 and the mechanism by which KNOX/BELL proteins regulate SAM development.

Introduction

Histone H3 lysine 27 tri-methylation (H3K27me3) marks an epigenetically transmitted state of repressed chromatin at thousands of loci in plant and animal genomes to prevent the ectopic activation of genes in cells where they are not required to be expressed (Schuettengruber et al., 2017; Yu

Received September 22, 2021. Accepted April 25, 2022. Advance access publication May 4, 2022

et al., 2019). The maintenance of H3K27me3 is essential for the stability of gene expression profiles in the same cell lineage (Comet et al., 2016). Polycomb repressive complex 2 (PRC2), which deposits H3K27me3, is a major effector of the maintenance of gene repression states across cell division and is thus essential for the establishment and propagation of cell identities (Reinberg and Vales, 2018). During cell differentiation and development, H3K27me3 is deposited in different genes. The mechanism by which PRC2 maintains or switches to new targets to establish H3K27me3-marked repressive chromatin domains remains unclear.

PRC2 is composed of three core subunits: E(Z) or EZH, which catalyzes H3K27me3 deposition; ESC or EED, which binds H3K27me3; and SU(Z)12, which functions as a scaffold (Zheng and Chen, 2011; Mozgova and Hennig, 2015; Laugesen et al., 2019; Yu et al., 2019). PRC2 has no specific DNA binding activity, and how it recognizes its target loci is not fully understood. In *Drosophila*, PRC2 is recruited by transcription factors to the so-called Polycomb Response Elements (PREs; Kassis and Brown, 2013). In mammals, PRC2 preferentially targets hypomethylated CpG-rich regions of genes (Blackledge et al., 2015). In *Arabidopsis thaliana*, several PRE-like elements have been identified, including a cis-element in *KNOTTED-LIKE HOMEOBOX* (*KNOX*) homeobox genes (Lodha et al., 2013), a cis-element in *LEAFY COTYLEDON2* (Berger et al., 2011), the RY element (CATGCA/TGCATG) in *FLOWERING LOCUS C* (Qüesta et al., 2016; Yuan et al., 2016), the gibberellic acid (GA) repeats (Deng et al., 2013), and the telobox present in many genes (Zhou et al., 2015; Xiao et al., 2017). The transcription factors BPC1, AZF1/TRB, and VAL1/2, which bind to GA repeats, telobox, and RY elements, respectively, recruit PRC2 proteins to their respective target loci in Arabidopsis (Xiao et al., 2017; Zhou et al., 2018; Yuan et al., 2020).

PRC2-mediated gene silencing is essential for key developmental processes in plants. Disruption of PRC2 genes leads to severe developmental defects, such as organ homeotic transformations, altered developmental-phase transitions, and cell differentiation/de-differentiation processes (Zheng and Chen, 2011; Mozgova and Hennig, 2015). For instance, Arabidopsis PRC2-mediated H3K27me3 is required for the repression of the meristem identity *KNOX1* genes, the meristem stem cell maintenance gene *WUSCHEL* (*WUS*), and root stem cell and meristem marker genes *WUS-LIKE HOMOEOBOX5* (*WOX5*) and *PLETHORA* during organ differentiation and meristem termination (Belles-Boix et al., 2006; Xu and Shen, 2008; Lafos et al., 2011; Sun et al., 2014). Consistently, mutations of the Arabidopsis PRC2 *E(Z)* genes *CURLY LEAF* (*CLF*)/*SWINGER* (*SWN*) and the *ESC* gene *FERTILIZATION-INDEPENDENT ENDOSPERM* result in the formation of masses of callus-like undifferentiated cells (Chanvivattana et al., 2004; Bouyer et al., 2011). In rice (*Oryza sativa*), knockdown of *PRC2* genes results in defects in both vegetative and reproductive apical meristem development (Liu et al., 2015a). Global differences in H3K27me3 distribution were detected between shoot apical meristem (SAM) and leaf tissues or inflorescence meristems in Arabidopsis and/or rice (Lafos et al., 2011; Liu et al., 2015a), which implies that PRC2 switches to different target loci to reprogram H3K27me3 during leaf organogenesis and meristem development.

KNOX proteins play important roles in SAM maintenance and cell differentiation. The *KNOX* genes are split into two classes, *KNOX1* and *KNOX2*. *KNOX1* genes are linked to the maintenance of meristem cell potential and to tissue proliferation, and their expression in leaves is implicated in leaf shape diversity (Hay and Tsiantis, 2010). In Arabidopsis, *KNOX1* genes promote cell proliferation in the SAM but are switched off in determinate leaf primordia (Long et al., 1996; Venglat et al., 2002; Belles-Boix et al., 2006; Hay and Tsiantis, 2010). Rice *KNOX1* genes have been functionally characterized, including *ORYZA SATIVA HOMEOBOX1* (*OSH1*), *OSH6*, *OSH15*, *OSH43*, and *OSH71* (Tsuda et al., 2011). The *osh1* null mutant has a defective SAM and shows arrested development at the three-leaf stage (Sato et al., 1996; Tsuda et al., 2011, 2014). In contrast, *KNOX2* genes promote tissue differentiation and play opposing rather than redundant roles with *KNOX1* genes in Arabidopsis (Furumizu et al., 2015).

KNOX and BEL-like (BELL) proteins belong to the Three Amino acid Loop Extension (TALE) homeodomain (HD) transcription factor family, which is conserved in all eukaryotic lineages (Mukherjee et al., 2009). Heterodimerization of KNOX with BELL proteins plays a pivotal role in regulating their transcription factor activities (Hay and Tsiantis, 2010). For instance, in Arabidopsis, the KNOX1 proteins STM, BP/KNAT1, and KNAT6 interact physically with the BELL protein REPLUMLESS to regulate meristem development (Smith and Hake, 2003). KNOX2 transcriptional activity also depends on the availability of the appropriate BELL partners (Furumizu et al., 2015). Interactions between BELL and KNOX proteins have been observed in other plant species, including rice (Yoon et al., 2017), barley (*Hordeum vulgare*; Müller et al., 2001), maize (*Zea mays*; Smith et al., 2002), potato (*Solanum tuberosum*; Chen et al., 2004), the moss *Physcomitrium patens* (Horst et al., 2016), and the liverwort *Marchantia polymorpha* (Dierschke et al., 2021) as well as in more ancestral species of the green lineage (Serikawa and Mandoli, 1999; Lee et al., 2008). KNOX proteins function as either positive or negative regulators of downstream targets. Their transcriptional function likely depends on the interacting BELL partners (Hackbusch et al., 2005; Pagnussat et al., 2007). However, the mechanism of the KNOX/BELL-regulated transcriptional switch of gene expression is unknown.

In this study, we uncovered the role of the coil-coiled protein PRC2-associated coiled-coil protein (PACP) in this mechanism in rice. PACP co-purified with PRC2 from rice shoot apex cells and interacted with both PRC2 core components and KNOX/BEL family proteins. PACP loss-of-function reduced genome-wide H3K27me3 and PRC2 binding and resulted in differential gene expression similar to that of PRC2 gene knockdown plants. Furthermore, PACP binding displayed a similar genomic profile to the binding of

the PRC2 core component EMF2b, and the top tier of PACP-binding regions was marked by H3K27me3. Therefore, we provide evidence for the PACP-dependent establishment or maintenance of PRC2-induced repression of cell differentiation-promoting genes targeted by KNOX1 in the rice SAM.

Results

Identification of PACP as a PRC2-interacting protein

The rice genome encodes two *E(Z)* homologs, *SDG711* and *SDG718*; 2 *ESC* homologs, *FIE1* and *FIE2*; and two *Su(Z)12* genes *EMF2a* and *EMF2b*. *FIE2* is highly expressed in rice vegetative tissues, while *FIE1* expression is only detected in endosperm, and its ectopic expression in vegetative tissues results in severe developmental defects (Zhang et al., 2012). To identify rice PRC2 complex proteins and potential PRC2-associated proteins, we produced transgenic rice plants expressing FLAG-tagged FIE2 protein under the control of the ubiquitin (*Ubi*) promoter. The *proUbi:FIE2-FLAG* (*FIE2-FLAG*) transgenic lines displayed no visible phenotype (Supplemental Figure S1A). We extracted total proteins from SAM tissues dissected from *FIE2-FLAG* transgenic and wild-type (WT) seedlings as previously described (Liu et al., 2015a), and performed immunoprecipitation (IP) with anti-FLAG antibody. The precipitated proteins were analyzed by mass spectrometry. Among the identified proteins (with at least two independent peptides detected in both replicates) were SDG711 and SDG718, EMF2b, the previously identified PRC2-associated protein OsVIL2 (Wang et al., 2013; Yang et al., 2013), and PCNA (proliferating-cell nuclear antigen), which was shown to interact with PRC2 in Arabidopsis (Jiang and Berger, 2017; Supplemental Data Set 1; Figure 1A). These data validated our approach to isolate PRC2 complex and PRC2-associated proteins from rice tissues.

Another protein (LOC_Os03g01840) was also identified as a PACP. To confirm the association of PACP with PRC2 and to study functional significance of this association in rice, we produced knockout (using clustered regularly interspaced short palindromic repeats [CRISPR]–CRISPR-associated protein 9 [CRISPR–Cas9] technology) or RNAi plants of *PACP*, *SDG711*, and *EMF2b* (Supplemental Figure S1, B–D), made antibodies against the SDG711, EMF2b, and PACP proteins (see "Materials and methods"; Supplemental Figure S2) and analyzed the proteins precipitated by anti-FLAG from *FIE2-FLAG* SAM protein extracts by immunoblotting. An antibody against the rice basic leucine zipper transcription factor 23 (bZIP23)(Zong et al., 2016) was used as a control. The analysis confirmed the presence of PACP, SDG711, and EMF2b, but not bZIP23, within the proteins precipitated by anti-FLAG (Figure 1B). In parallel, in a yeast two-hybrid (Y2H) library screening with SDG711 as bait, we also detected *PACP* cDNA as a positive clone. Tests of interactions between rice PACP and PRC2 components in Y2H confirmed the interaction of PACP with SDG711, SDG718, and EMF2b, but not with FIE2 or LHP1 (a PRC1-like component) (Figure 1C). BiFC assays in transiently transfected *Nicotiana benthamiana* cells confirmed the interaction of PACP with SDG711, SDG718, and EMF2b, as well as a weak interaction with FIE2 (Figure 1D).

Deletion analysis via Y2H revealed that the conserved C5 domain (located between the EZD1 and SANT domains) of SDG711 and both the ZnF-containing middle region and the VEFS (VRN2-EMF2-FIS2-Su[z]12) box-containing C-terminal end of EMF2b could interact with PACP (Figure 1E). PACP contains an N-terminal disordered region and a C-terminal coiled-coil region and is conserved in early land plants (Supplemental Figure S3; Figure 1E). Interestingly a PACP-like sequence was detected in charophytic algae but not in unicellular chlorophytes (Supplemental Figure S3). PACP could form a homodimer via N- to N- and C- to C-terminal domain interactions, and the C-terminal domain was required for its interaction with SDG711 (Figure 1E). The interaction between PACP and SDG711 or EMF2b was further confirmed by in vitro pull-down assays with *Escherichia coli*-produced His-tagged PACP and GST-tagged SDG711 and EMF2b proteins (Figure 1F). Together, these data indicate that PACP associates with PRC2 in rice cells.

PACP is important for rice SAM development and plant growth

The *pacp* mutant displayed reduced growth at the seedling and mature stages (Figure 2A), similar to the *SDG711* and *EMF2b* RNAi plants (Figure 2B; Supplemental Figure S1D; Liu et al., 2015b). The *pacp* mutation resulted in a flatter (with reduced depth between the SAM and the youngest leaf primordium) and smaller SAM (Figure 2C), reduced panicle (inflorescence meristem) size, and early flowering (Supplemental Figure S1E), which were also observed in the *SDG711* RNAi plants (Figure 2D; Liu et al., 2015b). The growth and SAM phenotypes of the *pacp* plants could be complemented by the genomic fragment of the *PACP* locus comprising the 3.1-kb promoter (*proPACP*) and the gene (*gPACP*), which was translationally fused with FLAG and HA sequences (*proPACP:gPACP–2xFLAG–2xHA*) (Supplemental Figure S1F; Figure 2, A and C). In situ hybridization of shoots detected *PACP* transcripts in the SAM and leaf primordia (Supplemental Figure S4A). Analysis of *proPACP:gPACP–GFP* and *proPACP–GUS* (Supplemental Figure S1F) transgenic plants indicated that *PACP* is expressed in both the shoots (vegetative and reproductive) and developing organs (e.g. leaf primordia and young leaves, tillers, stem nodes, and inflorescences) (Supplemental Figure S4, B and C). The expression pattern of this gene is consistent with the shoot developmental phenotypes of the mutants. These results indicate that *PACP* is required for rice shoot development and plant growth.

The PACP-dependent transcriptome overlaps with that of SDG711

To study whether PACP is involved in PRC2-dependent gene expression, we analyzed the transcriptomes of *pacp*,

A

Gene ID	FIE2-FLAG-1	FIE2-FLAG-2	CK-1	CK-2	Protein
LOC_Os08g04270	32	29	0	0	OsFIE2
LOC_Os03g19480	15	13	0	0	SDG718
LOC_Os06g16390	7	5	0	0	SDG711
LOC_Os02g56130	6	7	0	0	OsPCNA
LOC_Os02g05840	5	3	0	0	OsVIL2
LOC_Os09g13630	5	6	0	0	OsEMF2b
LOC_Os03g01840	3	3	0	0	PACP

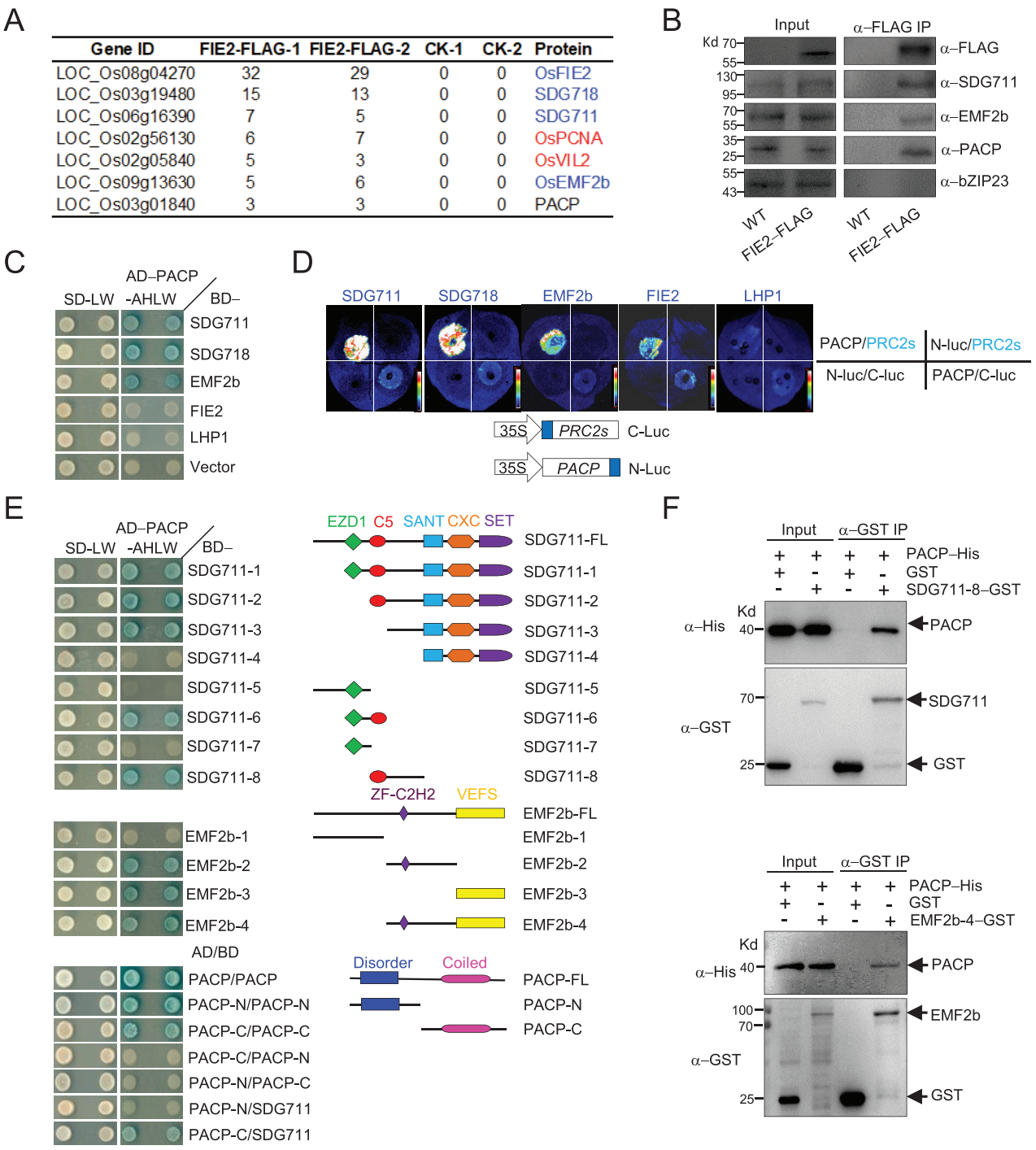

Figure 1 Identification of PACP as a PRC2-associated protein. A, Mass spectrometric identification of FLAG antibody affinity-purified proteins from the extracts of *FIE2–FLAG* SAM tissues (FIE2-FLAG). Extract from WT SAM tissues was used as a control (CK). Two biological repeats (separate experiments) were performed. The total numbers of identified unique peptides for each protein are indicated. B, Anti-FLAG Co-IP assays of proteins isolated from SAM tissues of *FIE2-FLAG* and WT plants. The precipitated proteins were analyzed by immunoblotting with the indicated antibodies. Anti-OsbZIP23 was used as a negative control. C, Y2H assay of the interactions of PACP with PRC2 proteins. The empty vector pGADT7 was used as a negative control. D, Split-luciferase complementation assay. *Nicotiana benthamiana* leaf cells were co-transformed with cLUC-tagged PRC2 proteins (SDG711, SDG718, EMF2b, FIE2, and LHP1) or cLUC alone with nLUC-tagged PACP or nLUC alone as shown. Diagrams of the constructs are shown on the right. E, Y2H assay of the truncated regions of PACP and PRC2 proteins. Full-length SDG711 (aa 1–896), SDG711-1 (aa 121–896), SDG711-2 (aa 249–896), SDG711-3 (aa 324–896), SDG711-4 (aa 523–896), SDG711-5 (aa 1–248), SDG711-6 (aa 121–323), SDG711-7 (aa 121–248), SDG711-8 (aa 249–522), EMF2b-FL (aa 1–604), EMF2b-1 (aa 1–207), EMF2b-2 (aa 208–452), EMF2b-3 (aa 453–604), EMF2b-4 (aa 208–604), PACP (aa 1–170), PACP-N (aa 1–76), and PACP-C (aa 77–170) were fused to the GAL4 BD or activation domain as indicated. Yeast cells were spotted onto stringent selection medium –WLHA with 40 μg mL^{-1} X-Gal or a nonselective medium –WL as a control. Right: Structures of SDG711, EMF2b, and PACP proteins. F, In vitro pull-down assay of the interaction between PACP and SDG711 or EMF2b. PACP–SUMO–6xHis was incubated with SDG711-8–GST, EMF2b-4–GST, or GST alone. Following pull down with GST beads, the eluates were analyzed by immunoblotting using the indicated antibodies.

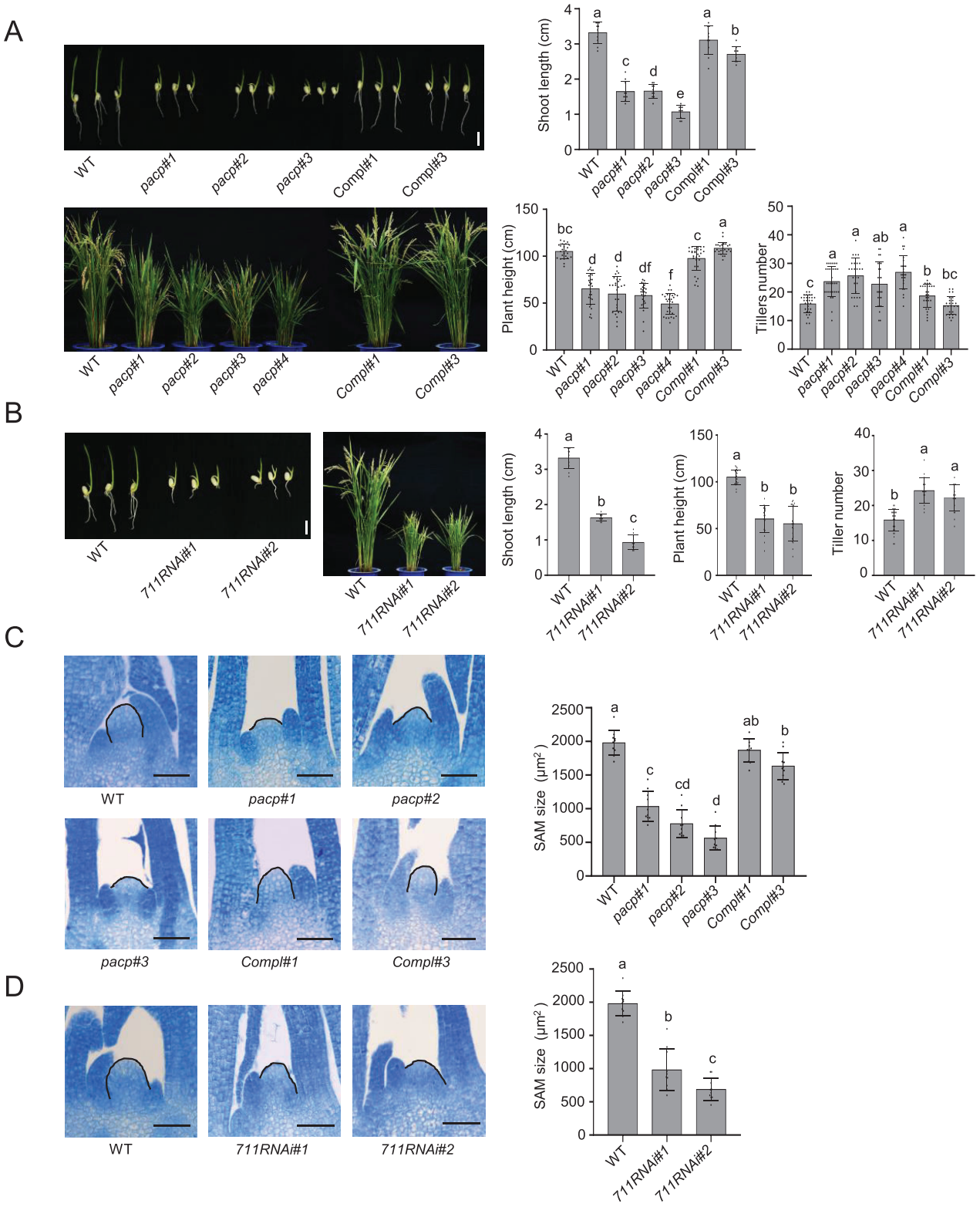

Figure 2 *PACP* is required for shoot development. A, Phenotypes of WT, *pacp* mutant, and complementation lines at 7 days after germination (DAG) (upper, Bar = 1 cm) and the mature (heading) stage (lower). Shoot lengths of seedlings (10 plants per line), mature plant height, and tiller number (>25 plants/line) of the different genotypes were measured (right). B, Phenotypes of WT and *SDG711* RNAi plants at 7 DAG (left, Bar = 1 cm) and the mature (heading) stage. The plant lengths and tiller number were measured as in (A). C, Shoot apex sections of WT, *pacp*, and complementation lines at 5 DAG. Bars = 50 μm. SAM size was determined by measuring the dome area delimited by drawing a straight line between the basal edges of the two opposing youngest leaf primordia. Ten plants per line were measured. D, Shoot apex sections of WT and *SDG711* RNAi lines at 5 DAG. Bar = 50 μm. SAM size was measured as in (C). Data represent the means ± SD (10 plants/line). Significance of differences (denoted by different letters) was tested by ANOVA.

SDG711 RNAi, and WT SAM tissues by RNA-seq. We harvested SAM tissues as previously described (Liu et al., 2015a) and validated the expression patterns of SAM and leaf primordia marker genes by reverse transcription-quantitative PCR (RT-qPCR) (Supplemental Figure S5A). Three biological replicates were performed for *pacp* and WT (see "Materials and methods"), and two replicates were performed for *SDG711* RNAi plants (Supplemental Figure S5B) (Supplemental Table S1). In the *pacp* SAM, we detected 1195 (>1.5-fold, false discovery rate [FDR] < 0.05) or 521 (>2-fold, FDR < 0.05) upregulated and 1,795 (>1.5-fold, FDR < 0.05) or 874 (>2-fold, FDR < 0.05) downregulated genes relative to the WT (Figure 3A; Supplemental Data Set 2). The upregulated genes were enriched for gene ontology (GO) functional categories related to metabolism or transcription, whereas the downregulated genes were more diverse (Supplemental Figure S5C). Transcription factor genes were over-represented among the differentially expressed genes (DEGs) of *pacp* (Figure 3B), among which the GRF, YABBY, LFY, RB, ZF-HD, TCP, E2F-DP, and OFP families were particularly enriched (Figure 3C).

In the *SDG711* RNAi SAM, we detected 1,205 (>1.5-fold, FDR < 0.05) or 840 (>2-fold, FDR < 0.05) upregulated and 787 (>1.5-fold, FDR < 0.05) or 395 (>2-fold, FDR < 0.05) downregulated genes relative to the WT (Figure 3D; Supplemental Data Set 2). The *SDG711* RNAi DEGs showed a high level of correlation ($R = 0.88$) with those detected in the *pacp* SAM (Figure 3E), with 331 of 1,205 upregulated and 459 of 787 downregulated DEGs (>1.5-fold) in *SDG711*RNAi plants overlapping with *pacp* DEGs (Figure 3, E and F). These results indicate that PACP and SDG711 play similar roles in regulating gene expression in the rice shoot apex.

The *pacp* mutation reduces genome-wide H3K27me3

To study whether the *pacp* mutation affected H3K27me3 in the SAM, we performed H3K27me3 ChIP-seq analysis of the *pacp* mutant and WT plants. Two replicates ($R > 0.85$) per genotype were performed (Supplemental Figure S6A; Supplemental Table S1). We identified 7,842 H3K27me3-marked peaks (7,689 genes) in *pacp* and 8,312 peaks (8,110 genes) in WT SAM (Supplemental Figure S6B). Pairwise scattering plots revealed 730 peaks with reduced (>1.5-fold, FDR < 0.01) H3K27me3 levels and 28 peaks with elevated H3K27me3 levels (>1.5-fold, FDR < 0.01) in the mutant (Supplemental Figure S6C). There were 900 genes that showed a decrease (>1.5-fold, FDR < 0.01) of H3K27me3 and 26 genes that displayed an increase in this mark (Supplemental Data Set 3). Metaplots confirmed the decreases in genic H3K27me3 genome wide (Supplemental Figure S6D). A moderate level of reverse correlation ($R = -0.33$) between H3K27me3 and gene expression changes was observed in the mutant (Supplemental Figure S6E), as observed previously (Liu et al., 2015a; Lu et al., 2020; Wang et al., 2021). We detected 156 upregulated genes that showed reduced H3K27me3 (>1.5-fold, FDR < 0.01) in the mutants, among which were many key genes that regulate meristem development (Supplemental Figure S6F; Supplemental Data Set 4).

The *pacp* mutation reduces PRC2 occupancy

To study whether the *pacp* mutation affects PRC2 recruitment, we used an anti-EMF2b antibody (which was of better quality than the anti-SDG711 antibody, Supplemental Figure S2), we performed ChIP-seq analysis of PRC2 binding in SAM tissues of WT and *pacp* plants. Two biological replicates per sample were performed (Supplemental Figure S7A; Supplemental Table S1). We detected 9,937 EMF2b-binding peaks (7,465 genes) in the WT SAM (Supplemental Figure S7B; Supplemental Data Set 5). Most EMF2b-binding peaks were located at proximal promoter regions (Supplemental Figure S7C). This result is consistent with the observation that most nucleation sites of H3K27me3 deposition are located at gene promoters in plants (Xiao et al., 2017). The EMF2b-binding genes were enriched for GO categories related to gene expression/transcription (Supplemental Figure S7D), corroborating the finding that PRC2 primarily targets transcription factor genes. More than 45% (4,502/9,937) of the EMF2b-binding peaks (or >37% of binding genes) overlapped with H3K27me3 peaks (Supplemental Figure S7, E and F). The levels of overlap between EMF2b binding and H3K27me3 were comparable to that observed for Arabidopsis PRC2 (Deng et al., 2013; Xiao et al., 2017). Interestingly, only peaks with the highest binding signals overlapped with H3K27me3, and the levels of H3K27me3 displayed the same trend as that of EMF2b binding (Supplemental Figure S7E).

In the *pacp* SAM, we detected 9,209 EMF2b-binding peaks and 6,918 genes (Supplemental Figure S7B). The *pacp* mutation reduced the overall EMF2b-binding signals (Figure 4, A and B). In the mutant, 1,471 peaks (1,518 genes) showed >1.5-fold (FDR < 0.01) decreases, but only 23 peaks (or 18 genes) displayed an increase in EMF2b binding (Figure 4C; Supplemental Data Set 5), indicating that the *pacp* mutation impaired the binding of EMF2b to a set of genomic targets. In addition, the effect of the *pacp* mutation on H3K27me3 was stronger in the regions bound by EMF2b than the unbound ones (Figure 4D; Supplemental Figure S7E). Approximately 47% (308/653) of the genes that showed reduced EMF2b binding in *pacp* lost H3K27me3 in the mutant (Figure 4E; Supplemental Figure S7G; Supplemental Data Set 5). These results indicate that PACP is involved in PRC2 binding and H3K27me3.

PACP-binding genes are enriched for H3K27me3 and overlap with those bound by EMF2b

To identify PACP-associated genes, we performed ChIP-seq analysis of the SAM tissues of plants complemented with anti-FLAG. Two replicates were performed (Supplemental Table S1). We identified 10,769 PACP-binding peaks (8,066 genes) (Figure 5A; Supplemental Data Set 6). These genes displayed much higher H3K27me3 levels than the genome-

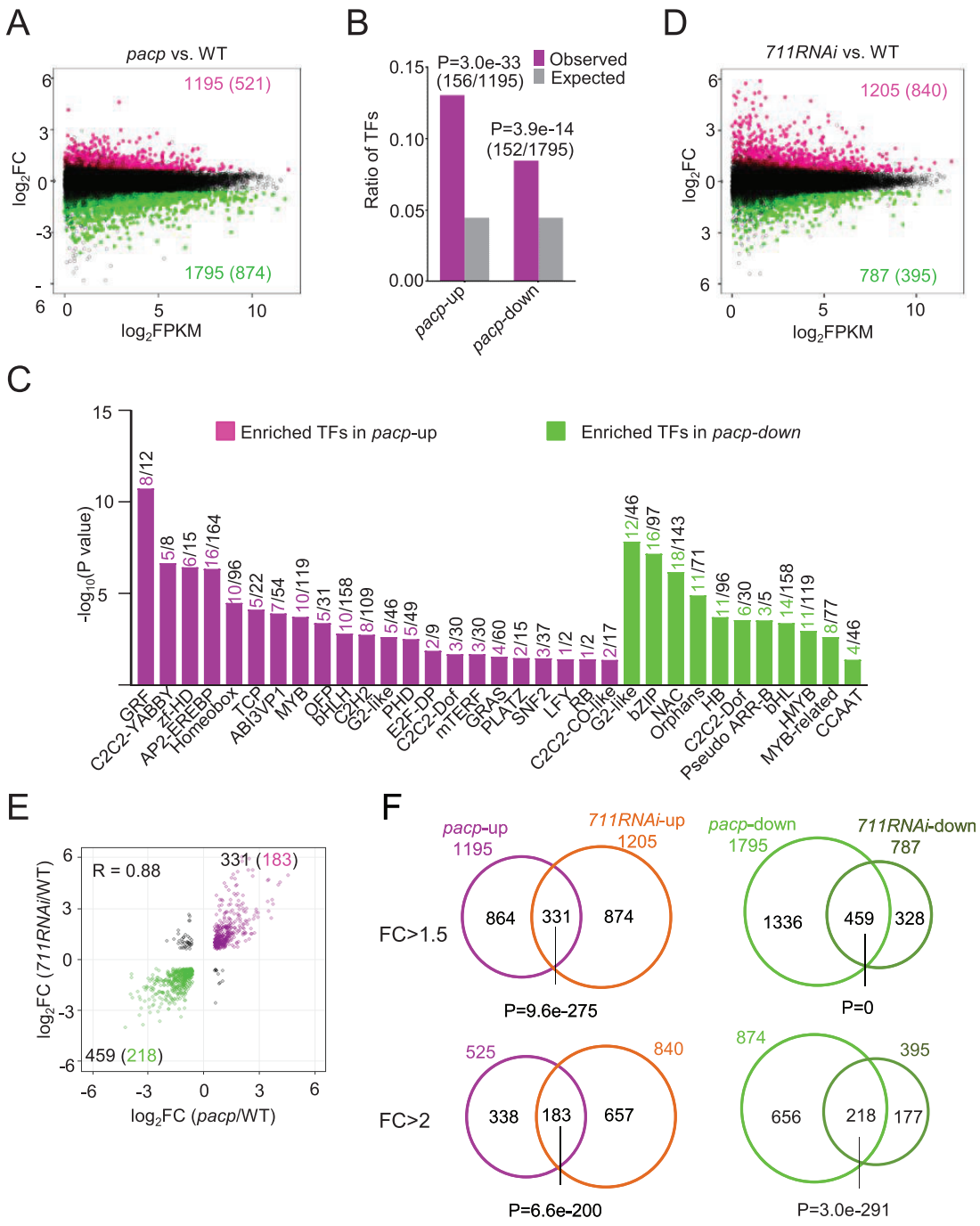

Figure 3 The *pacp* mutation has a similar effect as *SDG711* RNAi on the SAM transcriptome. A, Average read count plots of gene expression changes in *pacp* versus WT SAM. The *x* axis represents average gene expression level (FPKM), and the y axis represents $\log_2$ FPKM FC (*pacp*/WT). Significant [FDR < 0.05 and 1.5-FC or 2-FC (in parentheses)] upregulated and downregulated DEGs are indicated. B, Relative enrichment of transcription factor genes in the *pacp* DEGs. The frequency of transcription factor genes among upregulated or downregulated DEGs was compared with the expected genomic frequency. *P*-values were calculated using Fisher's test. C, Relative enrichments of transcription factor families among *pacp* DEGs. Detected gene number over the total gene number is indicated for each family. D, Average count plots of gene expression changes in *711RNAi* versus WT. Significant (FDR < 0.05 and 1.5-FC or 2 FC [in parentheses]) upregulated and downregulated DEGs are indicated. E, *pacp* DEGs positively correlated with *711RNAi* DEGs. The *x*-axis shows *pacp* DEGs, and the *y*-axis shows *711RNAi* DEGs. F, Venn diagrams showing the overlap between *pacp* and up and downregulated DEGs with FC > 1.5 and 2.0. *P*-values were calculated by hypergeometric test.

wide average (Figure 5B). The PACP-binding peaks showed a similar genomic distribution pattern as those of EMF2b (Figure 5A). There were 2,764 genes that were bound by both PACP and EMF2b (Supplemental Data Set 6). The top tier (3,239/10,769) of the PACP-binding peaks (the highest peaks with the broadest spread from the summit) also

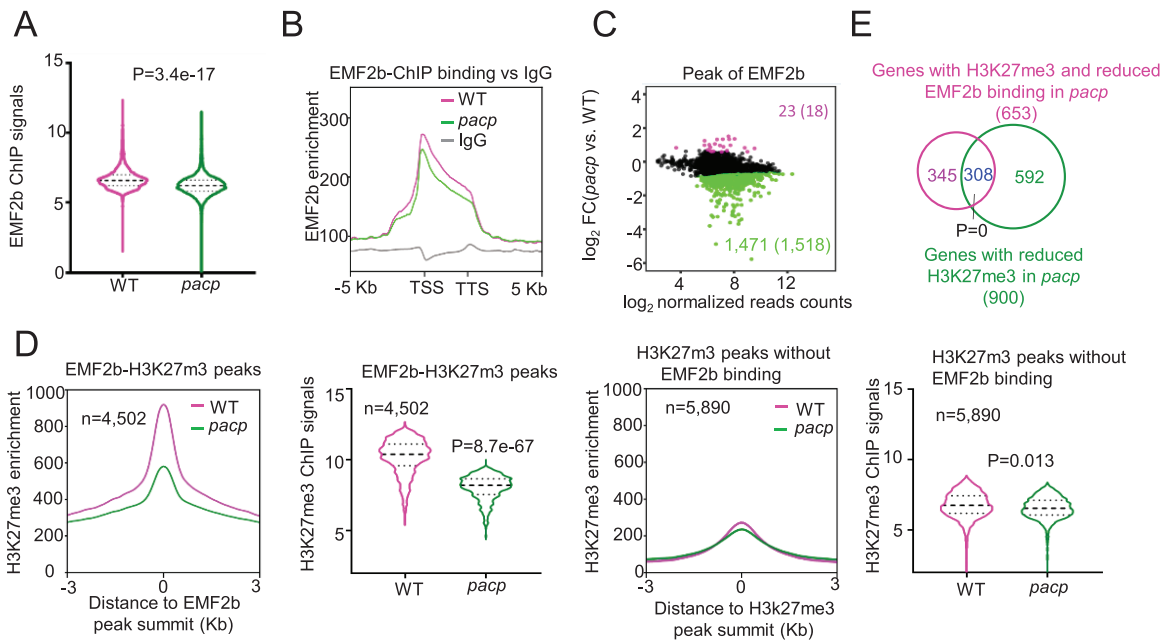

Figure 4 Loss of PACP leads to decreased EMF2b binding. A, Violin plots (with boxplots inside) of normalized EMF2b ChIP-seq read enrichment scores in WT and *pacp* SAM. The *P*-value for log2 normalized read counts between WT and *pacp* was calculated based on a two-sided Wilcoxon rank-sum test with Bonferroni correction. B, Metaplots of EMF2b-binding peaks in WT and *pacp*. C, Scatter plots of changes in EMF2b-binding in *pacp* versus WT. All EMF2b peaks (n = 9,937) were plotted. Significantly (FC > 1.5, FDR < 0.01) increased and reduced EMF2b binding peaks and numbers are indicated. D, Metaplots and violin plots of H3K27me3 levels of peaks with (left) and without (right) EMF2b binding in WT and *pacp*. The *P*-values were calculated based on a two-sided Wilcoxon rank-sum test with Bonferroni correction. E, Venn diagram showing the overlap between H3K27me3-marked genes with decreased EMF2b binding and genes with decreased H3K27me3 in *pacp* compared to the WT. The *P*-value was calculated by hypergeometric test.

showed the highest EMF2b binding and H3K27me3 signals (Figure 5A). In the *pacp* SAM, stronger decreases in H3K27me3 or EMF2b-binding levels were detected in the 3,239 common peaks than the regions not bound by PACP (Figure 5, C–D). The 3,239 common peaks corresponded to 1,289 genes that displayed concurrent (r = 0.47) decreases of both EMF2b binding and H3K27me3 in the *pacp* mutant (Figure 5E). Heatmap analysis revealed a cluster of 990 genes (C2) that clearly lost both EMF2b binding and H3K27me3 in the mutant (Figure 5F; Supplemental Data Set 6), 252 of which were upregulated in the mutant SAM (Figure 5G; Supplemental Data Set 6). Among these genes, many are known to be PRC2 targets and encode transcription factors that function in SAM development, including BLADE-ON-PETIOLE2 (BOP2), BOP3, YABBY4 (YAB4), YAB5, DROOPING LEAF (DL, a YABBY protein), MONOCULM1 (MOC1), CUC2, WOX7 (Figures 5, F and 6; Table 1). Collectively, these results indicate that PACP is required for PRC2 binding and H3K27me3 in the SAM.

PACP interacts with rice TALE HD transcription factors

A PACP ortholog in Arabidopsis was identified as a KNOX-binding protein (KNB36A) in an Y2H screening (Kollwig, 2010). The rice genome encodes seven KNOX1 and four KNOX2 proteins (Supplemental Figure S8). To investigate whether PACP interacts with KNOX proteins in rice, we tested the interaction of PACP with the seven KNOX1 (OSH1, OSH3, OSH6, OSH10, OSH14, OSH43, OSH71, and three of the four KNOX2 (OSH45, HOS59, and HOS66) proteins in Y2H assays. Rice WOX11 (Zhao et al., 2009) was also included in the tests. Except for WOX11, all of the tested proteins interacted with PACP (Figure 7A). The interactions were further confirmed by split luciferase assays in transiently transfected *N. benthamiana* leaf cells (Figure 7B). There are 14 BELL family proteins in rice (Supplemental Figure S8). PACP also interacted with the three tested BELL proteins (qSH1, qSH5, and OsHB86) in Y2H and split luciferase assays (Figure 7, A and B). These results indicate that PACP functions as an evolutionarily conserved TALE HD transcription factor-interacting protein.

KNOX proteins contain two repetitive domains (called KN1 and KN2) in addition to the conserved HD and the ELK domain (Figure 7C; Mukherjee et al., 2009). Deletion of the ELK, HD, or one of the KN domains of the rice KNOX1 protein OSH1 protein had no effect on its interaction with PACP (Figure 7C). However, the deletion of the two KN domains abolished the interaction (Figure 7C), indicating that one of the KN domains was sufficient for KNOX proteins to interact with PACP. The C-terminal domain of PACP was required for its interaction with OSH1 (Figure 7C). Pull-down experiments revealed in vitro interaction between *E. coli*-produced PACP-His and OSH1-MBP

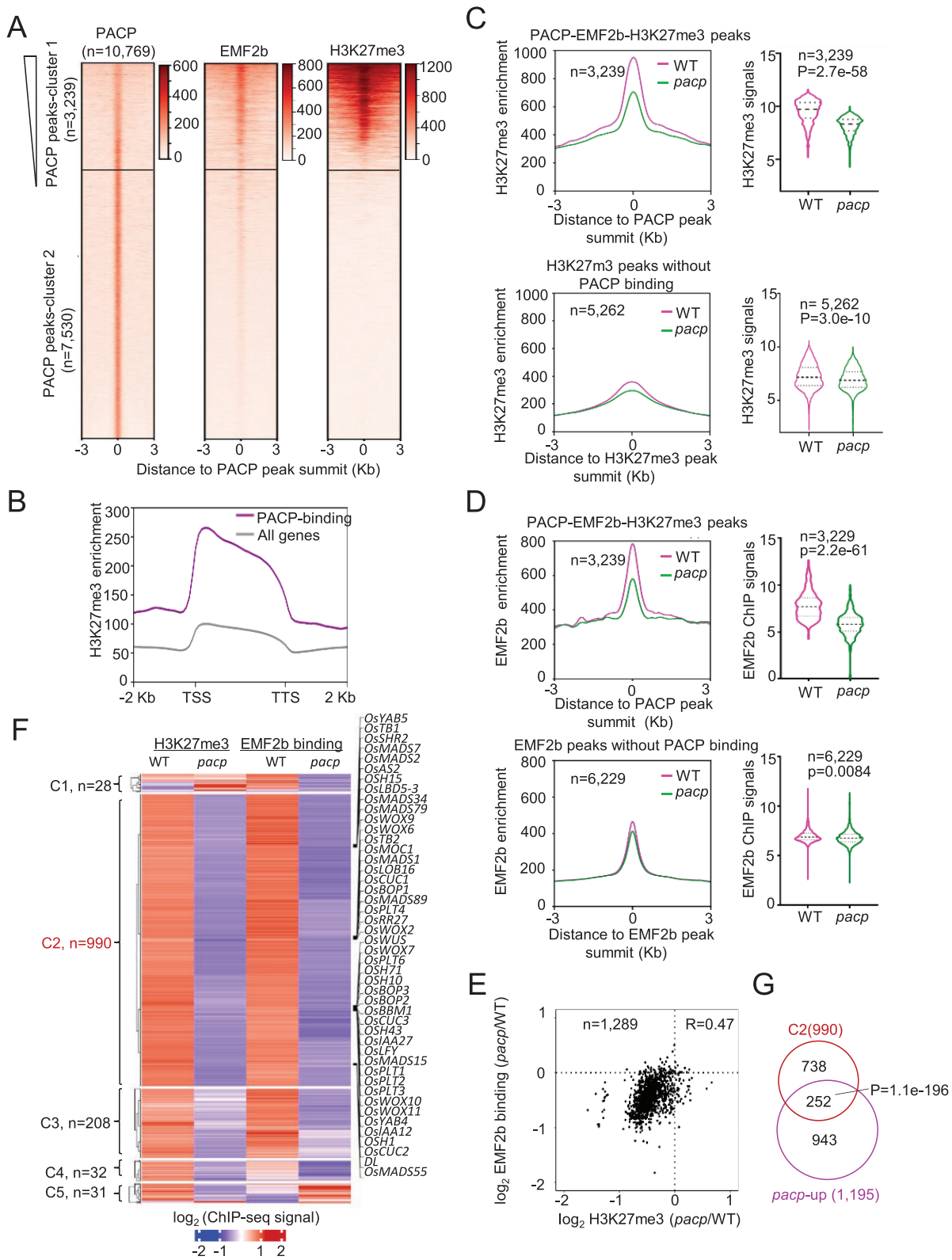

Figure 5 Identification of PACP-binding targets. A, Heatmaps of PACP and EMF2b binding and H3K27me3 signals at the PACP-binding peaks (n = 10,769). The top tier (3,239/10,769) PACP-binding peaks were bound by EMF2b and marked by H3K27me3. B, PACP-binding genes are highly enriched for H3K27me3 relative to the genomic average. C, Metaplots and violin plots of H3K27me3 levels of the 3,239 peaks commonly bound by EMF2b and PACP (upper) compared to those without PACP binding (lower) in WT and *pacp*. The *P*-value was calculated based on a two-sided Wilcoxon rank-sum test. D, Metaplots and violin plots of EMF2b-binding signals of the 3,239 commonly marked peaks (upper) compared to those without PACP binding (lower) in WT and *pacp*. The *P*-value was calculated based on a two-sided Wilcoxon rank-sum test. E, Correlation of changes between H3K27me3 and EMF2b binding levels of the 1,289 genes commonly marked by H3K27me3 and PACP and EMF2b binding (from 3,239 peaks) in *pacp* versus WT. F, Heatmaps of H3K27me3 and EMF2b-binding signals of the 1,289 genes in WT and *pacp*. Examples of target genes are shown on the right. G, Venn diagram showing the overlap between genes of cluster 2 of the heatmap (F) and upregulated DEGs in *pacp*.

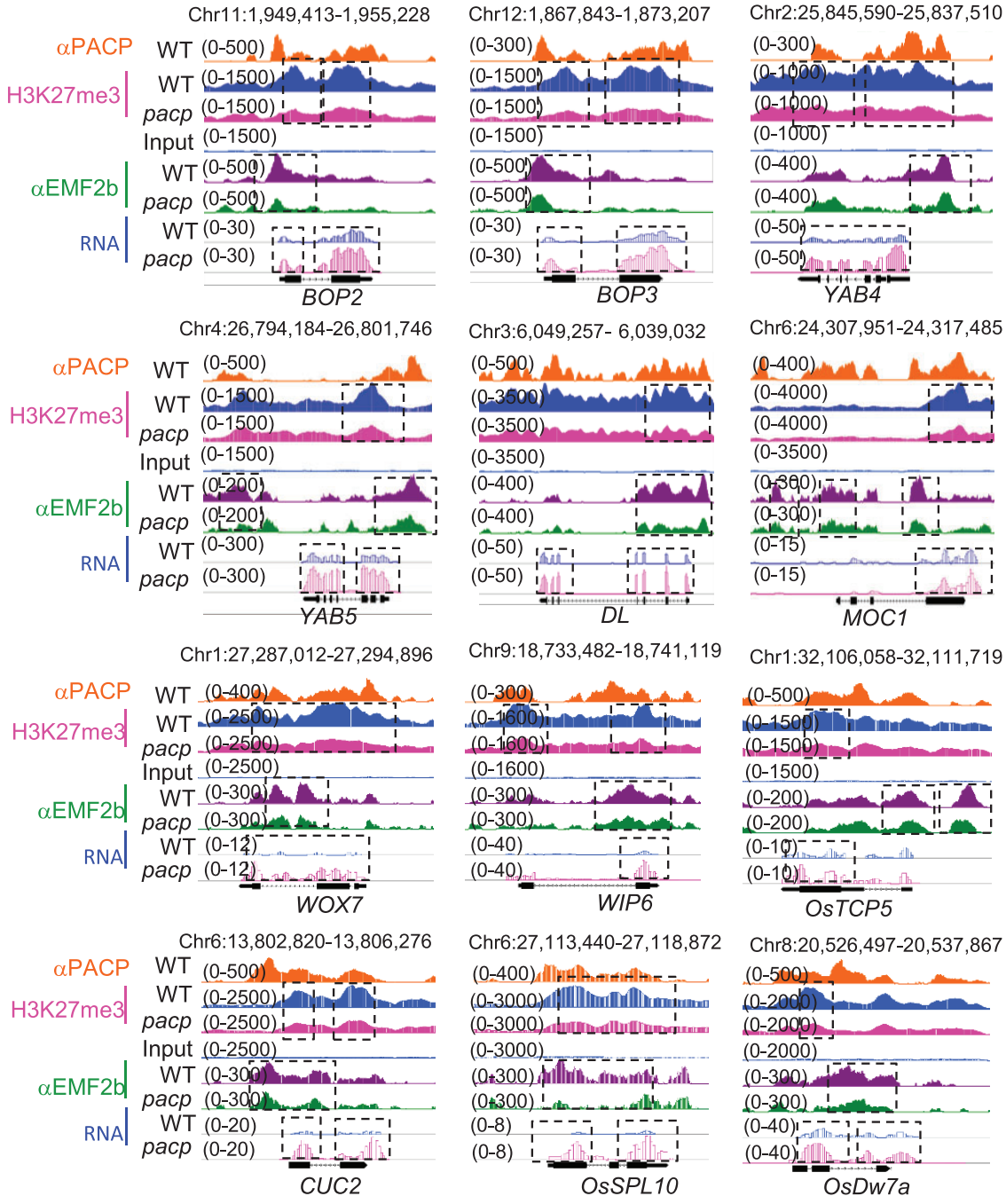

Figure 6 Integrative Genomics Viewer image of 12 transcription factor genes. PACP and EMF2b binding, H3K27me3, and RNA-seq data of 12 transcription factor genes selected from Table 1 in WT and *pacp*. The significant binding regions are indicated in black dotted boxes.

fusion proteins (Figure 7D). The interaction was further confirmed by Co-IP in *N. benthamiana* cells expressing PACP-GFP and OSH1-FLAG fusion proteins (Figure 7E). To test the in vivo interaction of OSH1 and PACP in rice plants, we collected SAM tissues from the *pacp* complementation plants (Supplemental Figure S1F; Figure 2) and subjected them to Co-IP with anti-FLAG antibody. The precipitated products were analyzed by anti-OSH1 produced as previously reported (Tsuda et al., 2014) (see "Materials and methods"; Supplemental Figure S2D). The results confirmed the in vivo interaction between OSH1 and PACP in rice SAM cells (Figure 7F).

PACP is involved in the repression of OSH1-targeted genes

The rice *KNOX1* gene *OSH1* is required for meristem development (Sato et al., 1996; Tsuda et al., 2014). OSH1 potentially targets 4,662 genes in young rice panicles (inflorescence meristems; Tsuda et al., 2014). In fact, many PACP-binding transcription factor genes that showed higher

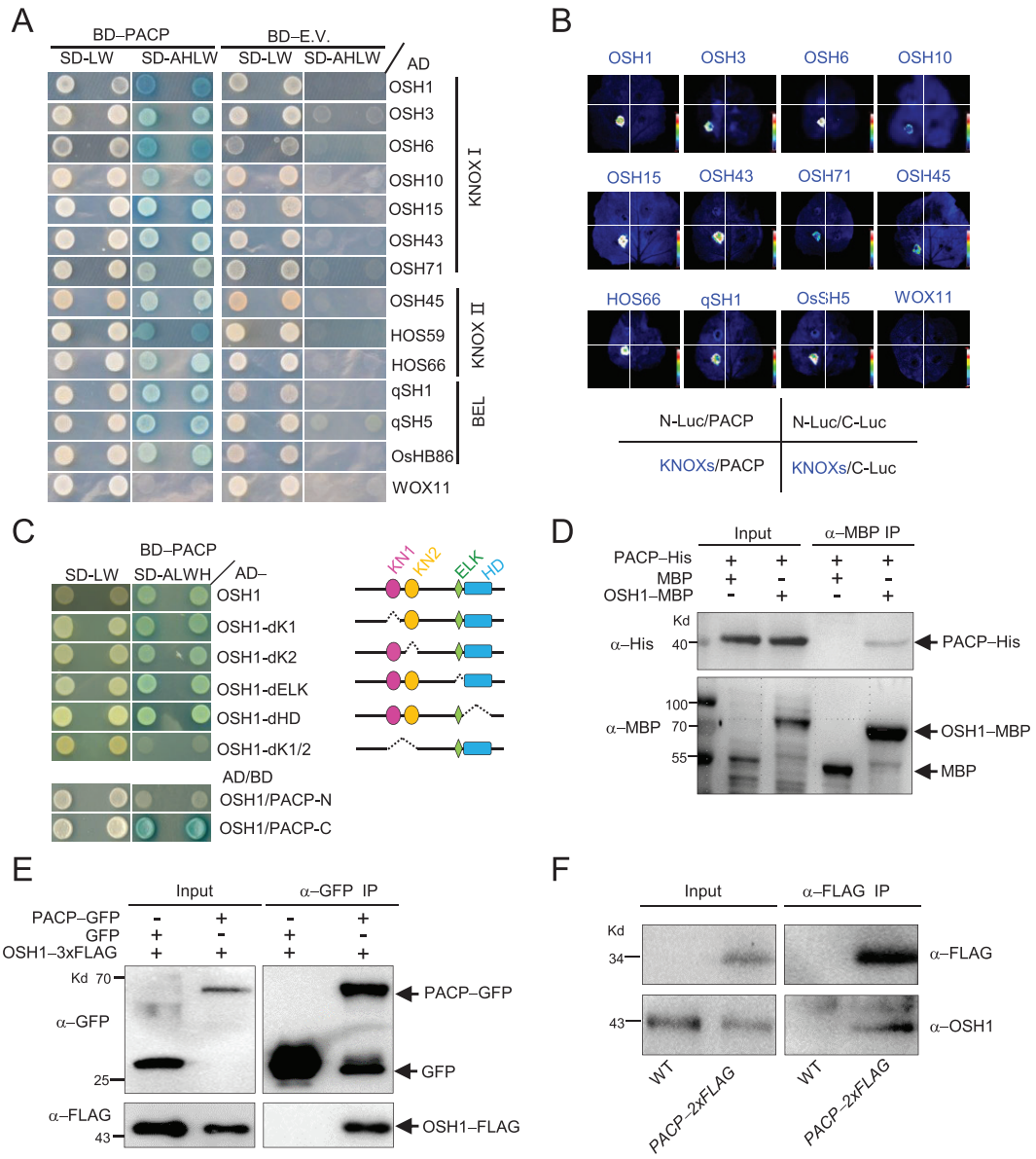

Figure 7 PACP interacts with KNOX and BELL proteins in vitro and in vivo. A, PACP interacts with KNOX and BELL proteins in an Y2H assay. WOX11 was used as a control. B, Split-luciferase complementation assay of the interactions of PACP with the indicated KNOX and BELL proteins. cLUC-tagged PACP or cLUC alone was co-transformed into *N. benthamiana* leaf cells with nLUC-tagged KNOX/BELL or nLUC alone. C, Y2H assay examining the interaction between the truncated regions of PACP and OSH1. The KN1 and KN2 domains of OSH1 and the C-terminus of PACP are required for this interaction. D, In vitro pull-down assay of the interaction of PACP with OSH1. Arrows mark the protein band as indicated. E, PACP interacts with OSH1 in *N. benthamiana* cells. The *35S:PACP–GFP* or *35S:GFP* vector was transiently co-transfected into *N. benthamiana* leaf cells with the *35S:OSH1–3xFLAG* vector. Total proteins were precipitated with anti-GFP beads. Anti-FLAG was used to detect OSH1 by immunoblotting. Arrows mark the protein band as indicated. F, PACP interacts with OSH1 in rice cells. Nuclei isolated from SAM tissue of 5-day-old WT and *Compl#1* (*PACP–2xFLAG*) seedlings were precipitated with anti-FLAG and analyzed by immunoblotting with anti-FLAG to detect PACP and with anti-OSH1 antibody to detect OSH1.

expression and lower H3K27me3 in the *pacp* mutant were also OSH1 targets (Table 1), among which *BOP2*, *BOP3*, *YAB4*, *YAB5*, *DL*, and *MOC1* encode known key regulators of leaf or floral organ development in rice. These genes are repressed in the vegetative SAM but expressed during lateral organogenesis (Ha et al., 2003; Li et al., 2003; Yamaguchi et al., 2004; Dai et al., 2007; Ohmori et al., 2008, 2011; Toriba and Hirano, 2014; Tanaka et al., 2017; Shao et al., 2019; Toriba et al., 2019; Figure 6). To confirm the function of PACP in regulating gene expression in the meristem and to validate the high-throughput data, we performed RT-qPCR, in situ hybridization, and chromatin immunoprecipitation with quantitative PCR (ChIP-qPCR) experiments. The RT-qPCR analysis validated the upregulation of the six OSH1 target genes in the *pacp* SAM (Figure 8A). The in situ hybridization revealed ectopic expression of *DL* and *YAB4* in

Table 1 PACP-binding transcription factor genes with reduced H3K27me3 and upregulated expression in the *pacp* SAM

Locus (TIGR)	TF family	Name	*pacp*-mRNA-level	*pacp*-H3K27me3-level	OSH1 binding[a]	Function
LOC_Os11g04600	TRAF	OsBOP2	Up	Down	Yes	Leaf initiation
LOC_Os12g04410	TRAF	OsBOP3	Up	Down	Yes	Leaf initiation
LOC_Os02g42950	C2C2-YABBY	OsYAB4	Up	Down	Yes	Inflorescence development
LOC_Os03g11600	C2C2-YABBY	DL	Up	Down	Yes	Meristem identity
LOC_Os04g45330	C2C2-YABBY	OsYAB5	Up	Down	Yes	Leaf initiation
LOC_Os06g40780	GRAS	MOC1	Up	Down	Yes	Tiller and panicle branches
LOC_Os01g47710	HB	OsWOX7	Up	Down	Yes	Tiller growth
LOC_Os04g51000	LFY	LFY	Up	Down	Yes	Inflorescence and floral meristem
LOC_Os01g66590	LOB	OsAS2	Up	Down	Yes	Shoot differentiation
LOC_Os03g11614	MADS	OsMADS1	Up	Down	Yes	Flower development
LOC_Os06g23650	NAC	CUC2	Up	Down	Yes	SAM
LOC_Os03g19900	AP2-EREBP	EREBP86	Up	Down	Yes	Unknown
LOC_Os06g36000	AP2-EREBP	OsERF122	Up	Down		Unknown
LOC_Os03g56050	AP2-EREBP	OsPLT7	Up	Down	Yes	Unknown
LOC_Os01g04800	AP2-EREBP	OsRAV2	Up	Down		Heading date and carpel development
LOC_Os06g33450	bHLH	OsbHLH054	Up	Down		Stomata development
LOC_Os09g31140	C2H2	OsWIP6	Up	Down		Unknown
LOC_Os08g39390	C2H2	OsDLN212	Up	Down		Unknown
LOC_Os08g33050	G2-like	OsMYB9c	Up	Down		Unknown
LOC_Os01g13740	G2-like	OsGLK2	Up	Down	Yes	Chlorophyll synthesis
LOC_Os08g08820	HB	Roc1	Up	Down		Epidermal cell fate
LOC_Os08g04190	HB	Roc7	Up	Down		Epidermal cell fate
LOC_Os08g33940	MYB	OsMYB31	Up	Down		Unknown
LOC_Os08g33800	MYB	OsDw7a	Up	Down	Yes	Unknown
LOC_Os01g12690	OFP	OsOFP1	Up	Down	Yes	Leaf angle and inflorescence development
LOC_Os05g36990	OFP	OsOFP14	Up	Down		Unknown
LOC_Os06g44860	SBP	OsSPL10	Up	Down		Trichome development
LOC_Os01g55750	TCP	OsTCP5	Up	Down		Unknown
LOC_Os08g37400	zf-HD	OsZHD2	Up	Down	Yes	Root meristem activity

[a]Tsuda et al. (2011).

the SAM and their upregulation in leaf primordia of *pacp* and *OSH1* RNAi plants (Song et al., 2018; Figure 8B), suggesting that PACP also represses *YAB4* in young leaves. ChIP-qPCR analysis validated the finding that H3K27me3 levels were reduced in different regions of the six genes in *pacp* but recovered in the complementation plants (Supplemental Figure S9, A and B). In addition, PACP binding to the six genes was verified by ChIP-qPCR analysis of the *pacp* complementation plants with anti-FLAG antibody (Supplemental Figure S9C). Finally, ChIP-qPCR analysis with anti-EMF2b antibody confirmed that PRC2 associated with *BOP2*, *BOP3*, *YAB4*, *YAB5*, *DL*, and *MOC1* and that the binding of EMF2b to these genes was reduced in *pacp* (Supplemental Figure S9D). These results indicate that PACP is involved in KNOX1-mediated repression of genes that promote lateral organ development by maintaining PRC2 binding and H3K27me3 in dividing cells of the rice SAM.

Discussion

In this study, we provided evidence that PACP is a PRC2-associated protein involved in PRC2 repression and H3K27me3 of a subset of genomic targets in the rice shoot apex. First, PACP was co-purified with PRC2 proteins from rice SAM protein extracts and interacted directly with PRC2 core components SDG711 and EMF2b. Second, a PACP loss-of-function mutation resulted in decreased H3K27me3 and EMF2b binding at a subset of genomic loci in the SAM, producing similar patterns of differential gene expression as *SDG711* RNAi plants. Finally, PACP and EMF2b displayed similar genomic binding profiles, and the genomic regions with the highest binding signals to both PACP and EMF2b showed high H3K27me3 levels. Thus, in addition to PCNA and VIL2 (Wang et al., 2013; Yang et al., 2013; Jiang and Berger, 2017; Figure 1A), plant PRC2 may associate with additional proteins to generate different PRC2 complexes, a situation resembling that in mammalian cells, where two distinct PRC2 holocomplexes (PRC2.1 and PRC2.2) have been identified (Kloet et al., 2016). Recent studies indicated that the PRC2.1 and PRC2.2 subunits regulate different gene sets and have distinct functions in maintaining and establishing, respectively, polycomb repression during mouse stem cell differentiation (Petracovici and Bonasio, 2021). The observation that only the binding regions with the highest and most widely spreading PACP and EMF2b-binding signals

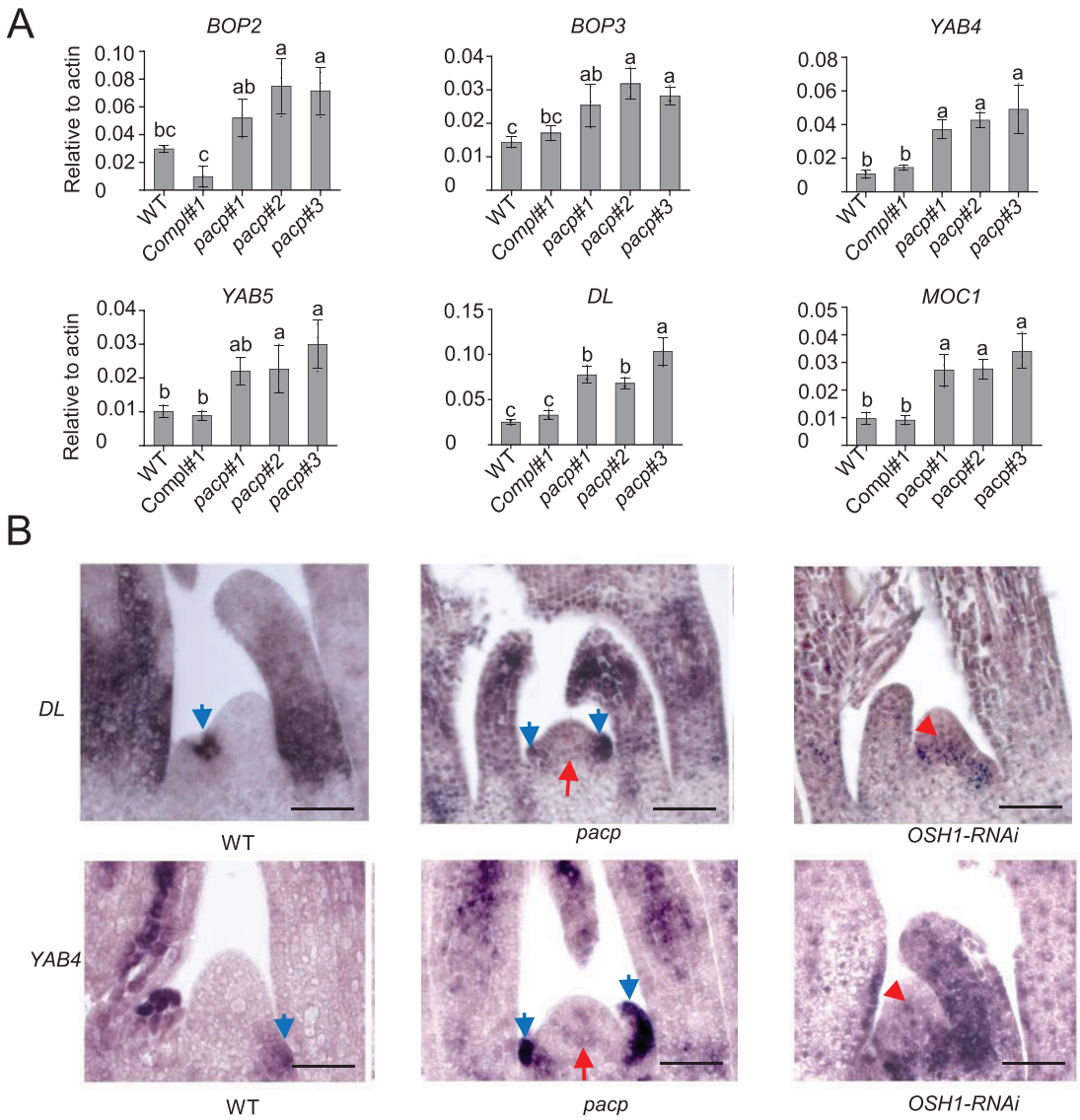

Figure 8 PACP represses the expression of lateral organ development-related genes in the SAM. A, RT-qPCR validation of the expression of the six genes in the SAM of WT, *pacp* mutants, and the complementation line. Data represent the means ± SD (three separate experiments per sample). Significance of differences (denoted by different letters) was tested by one-way ANOVA. B, In situ hybridization of *DL* and *YAB4* transcripts in the shoot apex of WT, *pacp* and *OSH1* RNAi plants. Arrows indicate signals in the SAM and leaf primordia. Bar = 50 μm.

co-localized with H3K27me3 suggests that PACP is likely involved in the stabilization, maintenance, or spreading of PRC2 and H3K27me3.

Unlike previously identified transcription factors involved in PRC2 recruitment in Arabidopsis (Xiao et al., 2017; Zhou et al., 2018; Yuan et al., 2020), PACP contains no DNA-binding domain (BD) but interacts with all of the tested TALE HD KNOX1, KNOX2, and BELL transcription factors. KNOX1 and KNOX2 proteins have a highly conserved DNA-BD and are thought to bind to the same cis-acting DNA elements (Furumizu et al., 2015). The most frequently found DNA-binding motif of the rice KNOX1 (OSH1) protein consists of two GA repeats separated by 3 bp, with G enriched in between Tsuda et al. (2014), which is similar to one of the previously identified PREs in Arabidopsis (Deng et al., 2013; Xiao et al., 2017). That the identified PACP motifs are similar to many transcription factor binding sites including that of KNOX (Supplemental Figure S10) suggests that PACP may also interact with other transcription factors for PRC2 recruitment or stabilization. We hypothesize that PACP is part of a rice PRC2 holocomplex that establishes and stabilizes PRC2 binding at a set of specific genes by interacting with DNA-binding transcription factors to maintain H3K27me3 and the repression of genes in dividing cells during shoot development.

In Arabidopsis, *KNOX1* and *KNOX2* genes play antagonistic roles in SAM activity and cell differentiation in leaf (or aerial) organs (Furumizu et al., 2015). KNOX1 proteins promote the pluripotency of meristem cells, directly activate the expression of the cytokinin biosynthetic isopentenyl transferase gene, and repress GA biosynthetic genes that promote leaf organogenesis and inflorescence development

(Yanai et al., 2005; Townsley et al., 2013). In rice, the loss of OSH1 function results in the absence of the SAM and reduced boundary depth between the SAM and the leaf primordium (Tsuda et al., 2014). The current finding that many OSH1-binding genes were derepressed and lost H3K27me3 in the *pacp* SAM indicates that PACP–PRC2 functions in the OSH1 pathway of gene repression to maintain meristem cell identity. This is consistent with the previous observation that leaf organogenesis and floral transition regulatory genes are marked by H3K27me3 and repressed in the SAM of Arabidopsis and rice plants (Lafos et al., 2011; Liu et al., 2015a). Because PACP is also expressed in young leaves and interacts with cell differentiation-promoting KNOX2, PACP-mediated PRC2 recruitment might also be involved in KNOX2-mediated gene repression during leaf organogenesis. The higher *YAB4* transcript levels detected by in situ hybridization in *pacp* leaf primordia (Figure 8B) support this hypothesis.

Although *KNOX1* and *KNOX2* play antagonistic roles in SAM activity and cell differentiation, there is no clear evidence of mutual repression between *KNOX1* and *KNOX2* (Furumizu et al., 2015). *KNOX1* genes are repressed by leaf organogenesis-promoting proteins. For instance, YABBY proteins required for leaf abaxial identity repress *KNOX1* gene expression in developing leaves in Arabidopsis by recruiting histone deacetylation enzymes (Chung et al., 2019). Similarly, BOP1 plays an important role in suppressing meristem activity in developing lateral organ primordia via the repression of *KNOX1* genes in Arabidopsis (Ha et al., 2003). In addition, *KNOX1* genes are repressed in leaves by the leaf organogenesis-promoting AS1, which directly recruits the PRC2 complex to these genes and maintains their repression (Lodha et al., 2013). The present data suggest a mutual repression between *KNOX1* and the leaf cell differentiation genes during meristem cell maintenance and differentiation.

KNOX1 and KNOX2 can function as either transcriptional activators or repressors (Hay and Tsiantis, 2010). The transcriptional activity of KNOX proteins is thought to depend on their interactions with BELL partners to form functional heterodimeric complexes (Winter et al., 2007; Furumizu et al., 2015). BELL genes also show tissue-specific expression in Arabidopsis. For instance, some BELL genes (e.g. *PNF* and *PNY*) are primarily expressed in the SAM, while others (such as *SAW1* and *SAW2*) are expressed in differentiating organs (Yu et al., 2009; Furumizu et al., 2015). Heterodimerization between KNOX and BELL proteins appears to be a highly selective process in vivo (Furumizu et al., 2015). It remains unclear whether the selective heterodimerization between KNOX and BELL proteins affects PACP binding and consequently PRC2 binding and H3K27me3 deposition to their targets, as KNOX/BELL heterodimers may interact with a third protein (Wang et al., 2007).

Materials and methods

Rice mutant and overexpression lines

In this study, all transgenic rice (*O. sativa*) lines were produced in the Zhonghua11 (ZH11) background. For the material used for immunoprecipitation followed by mass spectrometry (IP-MS) experiments, *FIE2–FLAG#1* and *FIE2–FLAG#2* were generated by transforming ZH11 rice with *proUbi:FIE2–3xFLAG* under the control of the maize (*Z. mays*) Ubi gene promoter. To produce knockdown lines of rice PRC2 genes, RNAi constructs (under the control of the 35S promoter) of *SDG711* and *EMF2b* were transformed into WT rice plants. The RNAi target region (214–644 bp) of *SDG711* is of high specificity. As *EMF2a* and *EMF2b* share highly similar coding sequences, the RNAi (674–1,086 bp) of *EMF2b* was designed to specifically knockdown the two *EMF2* genes.

The *pacp* mutant and *osh1* mutant were produced using a CRISPR–Cas9 system described in Gao and Zhao (2014). CRISPR-P (http://crispr.hzau.edu.cn/CRISPR2/) was used for gRNA design. The sequence CGAGCCAGGGGAGCGC GGGAGGG in *PACP* was selected as the specific target. The Gibson Assembly method (*Kpn* I digestion) was used to assemble the gRNA oligos into the CRISPR system.

To profile *PACP* gene expression, *proPACP:GUS* and *proPACP:gPACP–GFP* plants were generated. The −3,115- to + 556-bp region was selected as the predicted promoter sequence of *PACP*. For the *proPACP:GUS* construct, the promoter sequence was amplified in the *pCAMBIA1381-GUS* vector (Chu et al., 2006). For the *proPACP:gPACP–GFP* construct, the promoter combined with the genomic sequence of *PACP* (−3,115 to 1,067 bp, without the stop codon) was amplified and inserted into the pCAMBIA1300-GFP vector. To increase the flexibility of fusion with GFP, 3xGS linker (GGGGGS) was added. The complemention lines of *pacp* were produced by transforming *proPACP:gPACP–2xHA–2xFLAG* into *pacp* (Cas9 free) lines.

Plant growth

For sterile plant culture, rice seeds were surface sterilized with 75% ethanol (2 min) and 0.1% $HgCl_2$ (12 min) before sowing and were grown on 1/2 MS (Murashige and Skoog) solid medium (with 2.5 g L^{-1} Phytagel and 20 g L^{-1} sucrose) in sterilized tubes. All samples used for high-throughput sequencing and for phenotyping SAMs in seedlings were obtained from sterile cultures. Plants were grown in a growth chamber (SANYO Versatile Environmental Test Chamber # MLR-351H) under a 16-h light (approximately 15,000 lx)/8-h dark regime with a daytime temperature between 28°C and 32°C and nighttime temperature between 23°C and 26°C at 65% relative humidity. For field growth, germinated rice seedlings of all genotypes were transplanted to a field at the beginning of May and grown in Wuhan, China in the summer.

Polyclonal antibody preparation

Recombinant SDG711 (amino acids [aa] 300–550), EMF2b (aa 1–315), OSH1 (aa 1–238), and PACP (aa 1–108) proteins were used as antigens to produce polyclonal antibodies in rabbits. The recombinant antigen proteins were expressed and purified from *E. coli* DE3 cells (Yeasen Biotech, Shanghai, China; 11804ES80). After three cycles of injections, the

antisera were obtained, affinity-purified using antigen-coupled magnetic beads, and mixed with 20% glycerol for storage at −80°C.

Affinity purification and mass spectrometry

To identify PRC2-associated proteins, immuno-affinity purifications were performed as previously described, with minor modifications (Potok et al., 2019). Briefly, ∼10 g of SAM-enriched tissues were dissected from 7-day-old rice seedlings of *OE-FIE2-1* (3xFLAG tagged FIE2) and the WT (ZH11) as a negative control and crosslinked with 1.5 mM ethylene glycol-bis (Thermo Fisher Scientific, Waltham, MA, USA; 21565) for 30 min under a vacuum at room temperature. The crosslinked tissues were ground to a fine powder with a homogenizer (3 times, 1 min at 60 Hz min − 1) and suspended in 30 mL of IP buffer (50-mM Tris–Cl, pH 7.5, 150-mM NaCl, 5-mM $MgCl_2$, 10% glycerol, 0.1% NP-40, 0.5-mM DTT, 1-mM PMSF, 1× protease inhibitor cocktail from Roche, Basel, Switzerland). The samples were further homogenized until lump-free and centrifuged for 20 min at 4,000 *g* and 4°C. The lysates were filtered through two layers of Miracloth (Merck Millipore, Burlington, MA, USA; 475855) and the supernatants were incubated with 200 µL anti-FLAG M2 magnetic beads (M8823; Sigma St Louis, MO, USA) at 4°C for 3 h. The protein-bound beads were washed twice with 10 mL IP buffer, followed by six washes (5 min rotating at 4°C with 1.5-mL IP buffer), with a final wash with IP buffer without NP-40. The beads were submitted to Spec-Ally Company (Wuhan, China) for mass spectrometric analysis. Two independent replicates were performed.

Y2H assays

The cDNAs of the investigated genes were obtained by PCR. *SDG711*, *SDG718*, *EMF2b*, *FIE2*, *LHP1*, and *PACP* cDNAs were cloned into the *Bam HI* site of pGBK-T7, and *PACP*, *OSH1*, *OSH3*, *OSH6*, *OSH10*, *OSH15*, *OSH43*, *OSH71*, and *WOX11* cDNAs were cloned into the *Bam HI* site of pGADT7 (Clontech, Mountain View, CA, USA). Truncations of *SDG711*, *EMF2b*, *OSH1*, and *PACP* were obtained by PCR using specific primers. Yeast cells were spotted in stringent selection medium (synthetic dropout medium lacking Trp, Leu, His, and adenine (−WLHA)) with 40 µg/mL X-α-Gal or nonselective medium lacking Trp and Leu (−WL) as a control. All primers used are listed in Supplemental Data Set 7.

In vitro pull-down assay

To test the direct binding of PACP with PRC2 proteins and OSH1, in vitro pull-down assays were performed. SUMO-6xHis-tagged PACP was incubated with SDG711-8–GST and EMF2b-4–GST in GST beads and pulled down with GST beads (GE Healthcare, Chicago, IL, USA; 45-000-139). Mixtures of PACP-6xHis and MBP-OSH1 were pulled down from MBP-OSH1-conjugated beads (NEB E8037). The proteins were subsequently analyzed by immunoblotting. Anti-His antibody (Yeasen, Shanghai, China; 30404ES60) was used to detect PACP–6xHis. All proteins were expressed in *E. coli* BL21 (DE3) cells at 16°C.

Split-luciferase complementation assays

A split luciferase complementation assay with the pCAMBIA-nLUC and pCAMBIA-cLUC vectors was used to detect protein–protein interactions in *N. benthamiana* leaves (Chen et al., 2008). Firefly luciferase was divided into the N-terminal (nLUC) and C-terminal (cLUC) parts. SDG711, SDG718, EMF2b, FIE2, LHP1, OSH1, OSH3, OSH6, OSH10, OSH15, OSH43, OSH45, OSH71, PACP, qSH1, HOS66, OsSH5, and WOX11 were separately fused with nLUC in the pCAMBIA-nLUC vector. PACP was fused with cLUC in the pCAMBIA-cLUC vector. Agrobacterium strains transformed with the indicated nLUC and cLUC constructs were incubated, harvested, and resuspended in infiltration buffer (0.2-mM acetosyringone, 10-mM $MgCl_2$, and 10-mM MES) at identical concentrations (optical density at wavelength of 600nm [OD_{600}] = 1.0). Equal concentrations and volumes of Agrobacterium strains were mixed and co-infiltrated into *N. benthamiana* leaves with a needleless syringe. To prevent gene silencing, a construct encoding the viral p19 protein was infiltrated at the same time at an OD_{600} of 0.3. After infiltration, the plants were incubated at 24°C for 72 h before observation, and the leaves were injected with 0.15 mg mL^{-1} D-luciferin potassium salt as the substrate. The leaves were kept in the dark for 5 min before fluorescence observation. Luciferase activity was detected with a low-light cooled CCD (charge-coupled device) imaging apparatus (Tanon). The experiment was performed for three independent biological replicates (three separate experiments). All primers are listed in Supplemental Data Set 7.

Co-IP assay

For the in vivo Co-IP assays, approximately 10 g of the SAM tissues of 7-day-old seedlings was used. The FLAG-IP was eluted 3 times with 300 µL 250 µg mL^{-1} 3× FLAG peptides (Sigma; F4799) in TBS (50-mM Tris–Cl, pH 7.5, 150-mM NaCl) at 4°C. The 900 µL eluted solution was concentrated to ∼60 µL by freeze drying, resolved by SDS–PAGE (sodium dodecyl sulfate–polyacrylamide gel electrophoresis), and analyzed by immunoblotting using anti-FLAG monoclonal antibody (1:5,000 dilution) (Sigma-Aldrich, St Louis, MO, USA; F1804). The precipitated SDG711, EMF2b, and PACP proteins were detected using anti-SDG711 (at 1:3,000 dilution), anti-EMF2b (at 1:1,000 dilution), anti-bZIP23 (at 1:1,000 dilution), anti-OSH1 (at 1:1,000 dilution), and anti-PACP antibodies (1:1,000 dilution).

For co-IP in *N. benthamiana*, PACP–GFP and OSH1–3xFLAG were co-transformed into *N. benthamiana* leaves. At 72 h after transformation, the leaves were collected. IP and immunoblotting were performed as described above. Approximately 3 g leaf tissue and 100-µL GFP magnetic beads (AlpaLife, Shenzhen) were used for IP. The precipitated proteins were subjected to immunoblot analysis using anti-GFP (Abcam, Cambridge, UK; ab290; 1:1,000 dilution) and anti-FLAG (Sigma-Aldrich, F1804; 1:5,000 dilution) antibodies. The following horseradish peroxidase-conjugated

secondary antibody was used: Anti-mouse IgG (Abclonal, Woburn, MA, USA; AS003, 1:10,000).

Histological observation and in situ hybridization

For GUS histochemical staining, samples from *proPACP:GUS* T1 transgenic plants were stained in X-Gluc buffer (100-mM Na_3PO_4 pH 7, 10-mM EDTA, 0.1% Triton X-100, $K_3Fe(CN)_6$) at 37°C overnight. Ethanol (70%) was used to remove chlorophyll after GUS staining.

For GFP localization, *proPACP:gPACP-GFP* plants were fixed in 7% agarose (Roche) at 4°C for 15 min, and the shoots were sectioned transversally and longitudinally (50 μm) using a vibrating-blade microtome (Leica VT1200) and suspended in a drop of water on a covered glass slide. Sections were observed under a confocal laser scanning microscope (Leica TCS SP5) excited with a 488 nm Argon laser, and emission images were collected in the 500–560 nm range.

For histological analysis of the SAM, 5-day-old shoot apices were fixed in FAA fixative solution (formalin:acetic acid: 50% ethanol = 5:5:90) for 24 h at 4°C and dehydrated through a graded ethanol series from 70% to 100%. Images of SAMs were photographed under a microscope (Carl Zeiss, Oberkochen, Germany; Axio Scope.A1). SAM sizes were determined by measuring the dome area delimited by drawing a straight line between the basal edges of the two opposing youngest leaf primordia as described in http://www.bio-protocol.org/e2055. Ten SAMs per genotype were measured with ImageJ.

In situ hybridization was performed as previously reported (Liu et al., 2005). Briefly, 5-day-old shoots were fixed, dehydrated, embedded, sectioned, and mounted on slides. To prepare the digoxigenin-labeled RNA probes, specific coding regions of *PACP*, *DL*, *YAB4*, and *OSH1* were amplified via PCR using specific primers (Supplemental Data Set 7). Probe hybridization, posthybridization washing, and immunological detection of digoxigenin were performed successively. Images were photographed under a microscope (Carl Zeiss; Axio Scope.A1).

RNA extraction for RNA-seq

For RNA-seq samples, 2–3 mm shoot apices without leaf tissues were obtained from 5-day-old shoots with a scalpel under a dissecting microscope. Independent repeats from three *pacp* mutant lines, two *SDG711* RNAi lines, and WT were used. Approximately 30–50 apices per sample were harvested in liquid nitrogen for RNA extraction or RNA-seq. Total RNA was extracted using the TRIzol method (Invitrogen, Waltham, MA, USA; 15596-026).

RNA-seq and data analysis

RNA-seq libraries were constructed at the sequencing platform of Huazhong Agriculture University. Briefly, total RNA (5 μg per sample) was used to purify poly (A) mRNA, and this mRNA was used for the synthesis and amplification of cDNA. The libraries were prepared using a TruSeq RNA Sample Preparation Kit from Illumina and sequenced on an Illumina HiSeq 2000 system (paired-end, 2 × 150 bp).

Sequence reads were filtered using Trimmomatic version 0.36 (Bolger et al., 2014). The clean data were mapped against the MSU version 7.0 rice genome with the corresponding annotation by hisat2 using default parameters. These data were then analyzed for DEGs using Cufflinks (version 2.2.1) (Trapnell et al., 2014). Genes with an expression fold change (FC) > 1.5 with $P < 0.05$ were defined as differentially expressed. GO enrichment analysis of DEGs was performed on the agriGO website (http://systemsbiology.cau.edu.cn/agriGOv2/) and with adjusted $P < 0.05$ as the cutoff for significant GO terms.

ChIP

The Chromatin IP (ChIP) experiment was performed as described previously (Potok et al., 2019). Briefly, about 2 g of SAM-enriched tissue from 5-day-old seedlings was cross-linked in 1% formaldehyde for 30 min under a vacuum. Chromatin was extracted and fragmented to 200–500 bp by sonication (10–15 min sonication, 15/45 s on/off, at high energy level) with a Bioruptor Plus System (Diagenode) for H3K27me3 ChIP-seq or qPCR assays and 300–750 bp for EMF2b and PACP–FLAG. ChIP was performed using the following antibodies: H3K27me3 (8 μg, Merck Millipore, Burlington, MA, USA; 07-449), anti-EMF2b (12 μg), anti-IgG (12 μg; Abcam; ab37415), and anti-FLAG (12 μg; Sigma-Aldrich; F1804). The precipitated and input DNA samples were analyzed by high-throughput sequencing or by RT-PCR with gene-specific primers listed in Supplemental Data Set 7. The *pacp* mutant lines *pacp*#1, *pacp*#2, and WT were used as two independent biological repeats, respectively, in ChIP-seq. ChIP-qPCR assays were performed at least 3 times from two biological replicates.

ChIP-seq and data analysis

ChIP DNA libraries were prepared using a TruSeq DNA Sample Preparation Kit v2 (Illumina, San Diego, CA, USA). Briefly, 10 ng precipitated DNA was end-repaired, and a single "A" nucleotide was added to the 3′-end of the blunt ends of the fragments, followed by adapter ligation. Library fragments of 250–300 bp (insert plus adapter sequences) were isolated from an agarose gel, and PCR was performed with PCR primer cocktail to enrich the DNA fragments. After purification, the DNA fragments were sequenced with the Illumina HiSeq-2000 system.

Specifically, the quality of the ChIP-seq raw data (FASTQ files) was evaluated with FastQC (http://www.bioinformatics.babraham.ac.uk/projects/fastqc/), and the adaptors were trimmed from the raw reads with Trimmomatic version 0.36 (Bolger et al., 2014) with the arguments: ILLUMINACLIP:FA_ADAPTER:6:30:10 LEADING:3 TRAILING:3 MINLEN:36 SLIDINGWINDOW:4:15. The raw reads were mapped to the MSU7.0 genome with Bowtie2 (version 2.4.2) (Langmead and Salzberg, 2012) using default parameters. SAMtools were used to convert between SAM and BAM formats (samtools view) and to sort the BAM file (samtools sort; Li et al., 2009). Duplicate reads were removed with picard-tools (MarkDuplicates) using default settings (version

2.23.3; http://broadinstitute.github.io/picard/). The bam files were first converted to Wiggle files, and bigwig files were generated using bamCoverage with the parameters "–bam –binSize 10 –effectiveGenomeSize 4e8 –ignoreDuplicates –extendReads -normalizeUsing RPKM" in DeepTools (Ramirez et al., 2014), and the data were imported into the Integrated Genome Browser for visualization. The two replicates were merged using MACS2 in peak calling (version 2.2.6), for H3K27me3 with the parameters "-f BAM –broad –g 4e8 -q 0.01"; for EMF2b and PACP-FLAG with the parameters "-f BAM –g 4e8 -B -q e-5." The reads from input, IgG pull-down, and the WT were used as controls for H3K27me3, EMF2b, and PACP-FLAG ChIP-seq, respectively. H3K27me3 peaks were filtered for FC > 2.0 and counts >200. EMF2b and PACP-FLAG peaks were filtered for -log10 (q-value) > 5.0, FC > 3 and counts >200. The remaining peaks were subjected to subsequent analysis.

The ComputeMatrix and plotProfile programs of the DeepTools package were used to cluster the mean H3K27me3, EMF2b, and PACP levels at defined loci in the WT. The H3K27me3/EMF2b/PACP-positive regions in the WT were defined as H3K27me3/EMF2b/PACP-marked regions. ChIP target genes were identified using Bedtools with previously reported parameters (Yan et al., 2018); for EMF2b and PACP-FLAG, a peak summit (400 bp) that was positioned in the gene body or within 2-kb upstream of its transcription start site was considered to be a EMF2b or PACP-FLAG target gene; for H3K27me3, a gene overlapping at least one base pair with a peak region was assigned to the corresponding H3K27me3 marked gene. The ComplexHeatmap package (Gu et al., 2016) was used to build heatmaps of EMF2b and H3K27me3 ChIP-seq signals. The DiffBind (version 3.13) Bioconductor package (Ross-Innes et al., 2012) was used to find differential peaks between *pacp* and WT samples. The DESeq2 method implemented in DiffBind was used to test the differential peaks. FDR < 0.01 (adjusted *P*-value) and FC > 1.5 were used to define differential binding peaks. For EMF2b and PACP-FLAG de novo motif analysis, sequences were extracted from around peak summits and submitted to MEME software. The motif length was set to 6–12 bp, and the top 15 motifs are shown. Default settings were used for the other parameters.

RT-qPCR

One micrograms of total RNA was reverse-transcribed in a reaction volume of 20 μL using DNase and reverse transcriptase (Vazyme, Nanjing, China; R233-01) according to the manufacturer's instructions to obtain cDNA. RT-qPCR was performed as follows: 95°C for 10 s, 45 cycles of 95°C for 5 s, and 60°C for 40 s. Disassociation curve analysis was performed at 95°C for 15 s, 60°C for 20 s and 95°C for 15 s. Three biological replicates were performed (separate experiments), each with three technical repeats (three identical samples within an experiment). Data were collected using the ABI PRISM 7500 sequence detection system. The rice *ACTIN1* gene was used as the internal control. The primers used for RT-qPCR are listed in Supplemental Data Set 7.

Sequence alignment and phylogenetic analysis

Homologs of PACP were identified by performing BLAST searches of the protein sequences in Uniport. KNOX and BELL protein sequences in rice and Arabidopsis were previously identified (Mukherjee et al., 2009). The protein sequences were aligned with ClustalW (http://clustalw.ddbj.nig.ac.jp/) using the default settings, and the Clustal output files were submitted to GeneDoc (rbsc.org/gfx/genedoc) for visualization. A maximum-likelihood phylogenetic tree was generated using MEGAX (Kumar et al., 2018), with default values (substitution type: aa, substitution model: Jones–Taylor–Thornton, rates and patterns: uniform rates, gaps treatment: use all sites, ML heuristic method: Nearest-Neighbor-Interchange, initial tree for ML: default, branch swap filter: none, number of threads: 3). Protein alignment and machine-readable files of the phylogenetic analyses are as follows: PACP proteins, Supplemental Files S1 and S2; KNOX proteins, Supplemental Files S3 and S4; BELL proteins, Supplemental Files S5 and S6.

Statistical analysis

Statistical analyses were performed using GraphPad Prism version 7 (https://www.graphpad.com/scientific-software/prism/). For a two-group comparison, significance of differences was analyzed by Student's unpaired and two-tailed *t* tests with Welch's correction. For multiple comparisons, in case of equal standard deviations, one-way analysis of variance (ANOVA, nonparametric) tests were performed with Tukey's multiple comparisons. Statistical tests and the number of replicates are indicated in the figure legends; all statistical evidence is provided in Supplemental Data Set 8.

Accession numbers

Sequence data from this article can be found in the GenBank/EMBL libraries under the following accession numbers: *PACP (LOC_Os03g01840), FIE2 (LOC_Os08g04270), SDG711 (LOC_Os06g16390), SDG718 (LOC_Os03g19480, EMF2b (LOC_Os09g13630), EMF2a (LOC_Os04g08034), OsPCNA (LOC_Os02g56130),OsVIL2 (LOC_Os02g05840), OSH1 (LOC_Os03g51690), OSH3 (LOC_Os03g51710), OSH6 (LOC_Os01g19694), OSH10 (LOC_Os03g47016), OSH15 (LOC_Os07g03770), OSH43 (LOC_Os03g56110), OSH45 (LOC_Os08g19650), OSH71 (LOC_Os05g03884), HOS59 (LOC_Os06g43860), HOS66/OsKNAT7 (LOC_Os03g03164), qSH1 (LOC_Os01g62920), OsHB86 (LOC_Os10g39030), OsSH5 (LOC_Os05g38120), WOX11 (LOC_Os07g48560)*. The accession numbers of the Arabidopsis (TAIR) are as follows: *AtCLF (AT2G23380), AtSWN (AT4G02020), AtMEA (AT1G02580), AtSTM (AT1G62360), AtKNAT1 (AT4G08150), AtKNAT2 (AT1G70510), AtKNAT3 (AT5G25220), AtKNAT4 (AT5G11060), AtKNAT5 (AT4G32040), AtKNAT6 (AT1G23380), AtKNAT7 (AT1G62990) AtKNATM (AT1G14760), AtBEL1(At5g41410), AtBLH1(At2g35940), AtBLH3 (At1g75410), AtBLH4 (At2g23760), AtBLH5 (At2g27220), AtBLH6 (At4g34610),*

AtBLH7 (At2g16400), *AtBLH8 (At2g27990)*, *AtBLR (At5g02030)*, *AtBLH10 (At1g19700)*, *AtBLH11(At1g75430)*, and *ATH1 (AT4G32980)*. The accession numbers of the human genes are as follows: *HsEZH2* (Q15910).

The RNA-seq and ChIP-seq data described in this paper have been deposited in the SRA database (PRJNA758693). The mass spectrometry data have been deposited in the iProx database (accession number: IPX0004352000). Publicly available data sets used in this study are as follows: GSE68299 (H3K4me3), PRJNA296438 (H3K36me1, H3K36me2, and H3K36me3), GSE81436 (H3K9me2), GSE26734 (H3K4me2), GSE111308 (H3K9ac), GSE128434 (H3K4me1), GSE109616 (H3K27ac), and PRJNA380652 (H2A.Z).

Supplemental data

The following materials are available in the online version of this article.

Supplemental Figure S1. Production of transgenic and mutant plants.

Supplemental Figure S2. Test of antibodies produced in this study.

Supplemental Figure S3. PACP is evolutionarily conserved in land plants and charophytic algae.

Supplemental Figure S4. *PACP* expression pattern in shoots.

Supplemental Figure S5. RNA-seq analysis of *pacp* and WT SAM tissues.

Supplemental Figure S6. ChIP analysis of H3K27me3 in WT and *pacp* SAM tissues.

Supplemental Figure S7. ChIP-seq analysis of WT and *pacp* SAM tissues using anti-EMF2b antibody.

Supplemental Figure S8. The rice KNOX/BELL family.

Supplemental Figure S9. PACP is required for EMF2b binding and H3K27me3 of lateral organ development-related genes in the SAM.

Supplemental Figure S10. PACP-binding motifs correspond to transcription factor binding sites.

Supplemental Table S1. Summary of RNA-seq and ChIP-seq data.

Supplemental Data Set 1. Unique peptides identified by IP-MS.

Supplemental Data Set 2. DEGs in *pacp* and SDG711 RNAi compared to the WT.

Supplemental Data Set 3. Genes with decreased H3K27me3 levels in *pacp* compared to the WT.

Supplemental Data Set 4. Genes with upregulated expression and decreased H3K27me3 in *pacp*.

Supplemental Data Set 5. Genes with decreased EMF2b binding in *pacp* compared to the WT.

Supplemental Data Set 6. PACP-binding genes.

Supplemental Data Set 7. Primers used in this study.

Supplemental Data Set 8. Summary of statistical analyses.

Supplemental File S1. Multiple sequence alignments of PACP proteins.

Supplemental File S2. Machine-readable tree file of PACP proteins.

Supplemental File S3. Multiple sequence alignments of KNOX proteins.

Supplemental File S4. Machine-readable tree file of KNOX proteins.

Supplemental File S5. Multiple sequence alignments of BELL proteins.

Supplemental File S6. Machine-readable tree file of BELL proteins.

Funding

This work was supported by National Natural Science Foundation of China [31730049, 32070563, and 31970806] and the Fundamental Research Funds for the Central Universities [2662015PY228]. We thank Qinglu Zhang for help with field experiments and Dr Shiyong Song for providing *OSH1* RNAi seeds.

Conflict of interest statement. The authors declare that they have no competing interests.

References

Belles-Boix E, Hamant O, Witiak SM, Morin H, Traas J, Pautot V (2006) *KNAT6*: an *Arabidopsis* homeobox gene involved in meristem activity and organ separation. Plant Cell **18**: 1900–1907

Berger N, Dubreucq B, Roudier F, Dubos C, Lepiniec L (2011) Transcriptional regulation of *Arabidopsis LEAFY COTYLEDON2* involves *RLE*, a *cis*-element that regulates trimethylation of histone H3 at lysine-27. Plant Cell **23**: 4065–4078

Blackledge NP, Rose NR, Klose RJ (2015) Targeting Polycomb systems to regulate gene expression: modifications to a complex story. Nat Rev Mol Cell Biol **16**: 643–649

Bolger AM, Lohse M, Usadel B (2014) Trimmomatic: a flexible trimmer for Illumina sequence data. Bioinformatics **30**: 2114–2120

Bouyer D, Roudier F, Heese M, Andersen ED, Gey D, Nowack MK, Goodrich J, Renou JP, Grini PE, Colot V, et al (2011) Polycomb repressive complex 2 controls the embryo-to-seedling phase transition. PLoS Genet **7**: e1002014

Chanvivattana Y, Bishopp A, Schubert D, Stock C, Moon YH, Sung ZR, Goodrich J (2004) Interaction of Polycomb-group proteins controlling flowering in *Arabidopsis*. Development **131**: 5263–5276

Chen H, Banerjee AK, Hannapel DJ (2004) The tandem complex of BEL and KNOX partners is required for transcriptional repression of *ga20ox1*. Plant J **38**: 276–284

Chen HM, Zou Y, Shang YL, Lin HQ, Wang YJ, Cai R, Tang XY, Zhou JM (2008) Firefly luciferase complementation imaging assay for protein-protein interactions in plants. Plant Physiol **146**: 368–376

Chu ZH, Yuan M, Yao LL, Ge XJ, Yuan B, Xu CG, Li XH, Fu BY, Li ZK, Bennetzen JL, et al (2006) Promoter mutations of an essential gene for pollen development result in disease resistance in rice. Genes Dev **20**: 1250–1255

Chung Y, Zhu Y, Wu MF, Simonini S, Kuhn A, Armenta-Medina A, Jin R, Østergaard L, Gillmor CS, Wagner D (2019) Auxin Response Factors promote organogenesis by chromatin-mediated repression of the pluripotency gene *SHOOTMERISTEMLESS*. Nat Commun **10**: 886

Comet I, Riising EM, Leblanc B, Helin K (2016) Maintaining cell identity: PRC2-mediated regulation of transcription and cancer. Nat Rev Cancer **16**: 803–810

Dai MQ, Hu YF, Zhao Y, Liu HF, Zhou DX (2007) A *WUSCHEL-LIKE HOMEOBOX* gene represses a *YABBY* gene expression required for rice leaf development. Plant Physiol **144**: 380–390

Deng W, Buzas DM, Ying H, Robertson M, Taylor J, Peacock WJ, Dennis ES, Helliwell C (2013) *Arabidopsis* polycomb repressive complex 2 binding sites contain putative GAGA factor binding motifs within coding regions of genes. BMC Genom **14**: 593

Dierschke T, Flores-Sandoval E, Rast-Somssich MI, Althoff F, Zachgo S, Bowman JL (2021) Gamete expression of TALE class HD genes activates the diploid sporophyte program in *Marchantia polymorpha*. Elife **10**: e57088

Furumizu C, Alvarez JP, Sakakibara K, Bowman JL (2015) Antagonistic roles for *KNOX1* and *KNOX2* genes in patterning the land plant body plan following an ancient gene duplication. PLoS Genet **11**: e1004980

Gao YB, Zhao YD (2014) Self-processing of ribozyme-flanked RNAs into guide RNAs *in vitro* and *in vivo* for CRISPR-mediated genome editing. J Integr Plant Biol **56**: 343–349

Gu Z, Eils R, Schlesner M (2016) Complex heatmaps reveal patterns and correlations in multidimensional genomic data. Bioinformatics **32**: 2847–2849

Ha CM, Kim GT, Kim BC, Jun JH, Soh MS, Ueno Y, Machida Y, Tsukaya H, Nam HG (2003) The *BLADE-ON-PETIOLE 1* gene controls leaf pattern formation through the modulation of meristematic activity in *Arabidopsis*. Development **130**: 161–172

Hackbusch J, Richter K, Müller J, Salamini F, Uhrig JF (2005) A central role of *Arabidopsis thaliana* ovate family proteins in networking and subcellular localization of 3-aa loop extension homeodomain proteins. Proc Natl Acad Sci USA **102**: 4908–4912

Hay A, Tsiantis M (2010) KNOX genes: versatile regulators of plant development and diversity. Development **137**: 3153–3165

Horst NA, Katz A, Pereman I, Decker EL, Ohad N, Reski R (2016) A single homeobox gene triggers phase transition, embryogenesis and asexual reproduction. Nat Plants **2**: 15209

Jiang D, Berger F (2017) DNA replication–coupled histone modification maintains Polycomb gene silencing in plants. Science **357**: 1146–1149

Kassis JA, Brown JL (2013) Chapter three-polycomb group response elements in *Drosophila* and Vertebrates. *In* T Friedmann, JC Dunlap, SF Goodwin, eds, Advances in Genetics. Academic Press, Cambridge, MA, pp 83–118

Kloet SL, Makowski MM, Baymaz HI, van Voorthuijsen L, Karemaker ID, Santanach A, Jansen PWTC, Di Croce L, Vermeulen M (2016) The dynamic interactome and genomic targets of Polycomb complexes during stem-cell differentiation. Nat Struct Mol Biol **23**: 682–690

Kollwig G (2010) How to Bridle a Homeodomain Protein: Characterization of At KNB36 and At MPB2C. University of Vienna, Vienna, Austria

Kumar S, Stecher G, Li M, Knyaz C, Tamura K (2018) MEGA X: molecular evolutionary genetics analysis across computing platforms. Mol Biol Evol **35**: 1547–1549

Lafos M, Kroll P, Hohenstatt ML, Thorpe FL, Clarenz O, Schubert D (2011) Dynamic regulation of H3K27 trimethylation during *Arabidopsis* differentiation. PLoS Genet **7**: e1002040

Langmead B, Salzberg SL (2012) Fast gapped-read alignment with Bowtie 2. Nat Methods **9**: 357–359

Laugesen A, Højfeldt JW, Helin K (2019) Molecular mechanisms directing PRC2 recruitment and H3K27 methylation. Mol Cell **74**: 8–18

Lee JH, Lin HW, Joo S, Goodenough U (2008) Early sexual origins of homeoprotein heterodimerization and evolution of the plant KNOX/BELL family. Cell **133**: 829–840

Li H, Handsaker B, Wysoker A, Fennell T, Ruan J, Homer N, Marth G, Abecasis G, Durbin R, Proc GPD (2009) The sequence alignment/map format and SAMtools. Bioinformatics **25**: 2078–2079.

Li XY, Qian Q, Fu ZM, Wang YH, Xiong GS, Zeng DL, Wang XQ, Liu XF, Teng S, Hiroshi F, et al (2003) Control of tillering in rice. Nature **422**: 618–621

Liu HJ, Wang SF, Yu XB, Yu J, He XW, Zhang SL, Shou HX, Wu P (2005) ARL1, a LOB-domain protein required for adventitious root formation in rice. Plant J **43**: 47–56

Liu X, Zhou S, Wang W, Ye Y, Zhao Y, Xu Q, Zhou C, Tan F, Cheng S, Zhou DX (2015a) Regulation of histone methylation and reprogramming of gene expression in the rice inflorescence meristem. Plant Cell **27**: 1428–1444

Liu X, Zhou S, Wang W, Ye Y, Zhao Y, Xu Q, Zhou C, Tan F, Cheng S, Zhou DX (2015b) Regulation of histone methylation and reprogramming of gene expression in the rice inflorescence meristem. Plant cell **27**: 1428–1444

Lodha M, Marco CF, Timmermans MC (2013) The ASYMMETRIC LEAVES complex maintains repression of KNOX homeobox genes via direct recruitment of Polycomb-repressive complex2. Genes Dev **27**: 596–601

Long JA, Moan EI, Medford JI, Barton MK (1996) A member of the KNOTTED class of homeodomain proteins encoded by the *STM* gene of *Arabidopsis*. Nature **379**: 66–69

Lu Y, Tan F, Zhao Y, Zhou SL, Chen XS, Hu YF, Zhou DX (2020) A Chromodomain-Helicase-DNA-Binding factor functions in chromatin modification and gene regulation. Plant Physiol **183**: 1035–1046

Müller J, Wang Y, Franzen R, Santi L, Salamini F, Rohde W (2001) *In vitro* interactions between barley TALE homeodomain proteins suggest a role for protein–protein associations in the regulation of *Knox* gene function. Plant J **27**: 13–23

Mozgova I, Hennig L (2015) The polycomb group protein regulatory network. Ann Rev Plant Biol **66**: 269–296

Mukherjee K, Brocchieri L, Bürglin TR (2009) A comprehensive classification and evolutionary analysis of plant homeobox genes. Mol Biol Evol **26**: 2775–2794

Ohmori Y, Abiko M, Horibata A, Hirano HY (2008) A transposon, *Ping*, is integrated into intron 4 of the *DROOPING LEAF* gene of rice, weakly reducing its expression and causing a mild drooping leaf phenotype. Plant Cell Physiol **49**: 1176–1184

Ohmori Y, Toriba T, Nakamura H, Ichikawa H, Hirano HY (2011) Temporal and spatial regulation of *DROOPING LEAF* gene expression that promotes midrib formation in rice. Plant J **65**: 77–86

Pagnussat GC, Yu HJ, Sundaresan V (2007) Cell-fate switch of synergid to egg cell in *Arabidopsis eostre* mutant embryo sacs arises from misexpression of the BEL1-like homeodomain Gene *BLH1*. Plant Cell **19**: 3578–3592

Petracovici A, Bonasio R (2021) Distinct PRC2 subunits regulate maintenance and establishment of Polycomb repression during differentiation. Mol Cell **81**: 2625–2639

Potok ME, Wang YF, Xu LH, Zhong ZH, Liu WL, Feng SH, Naranbaatar B, Rayatpisheh S, Wang ZH, Wohlschlegel JA, et al (2019) *Arabidopsis* SWR1-associated protein methyl-CpG-binding domain 9 is required for histone H2A.Z deposition. Nat Commun **10**: 3352

Qüesta JI, Song J, Geraldo N, An H, Dean C (2016) *Arabidopsis* transcriptional repressor VAL1 triggers Polycomb silencing at *FLC* during vernalization. Science **353**: 485–488

Ramirez F, Dundar F, Diehl S, Gruning BA, Manke T (2014) deepTools: a flexible platform for exploring deep-sequencing data. Nucleic Acid Res **42**: W187–W191

Reinberg D, Vales LD (2018) Chromatin domains rich in inheritance. Science **361**: 33–34

Ross-Innes CS, Stark R, Teschendorff AE, Holmes KA, Ali HR, Dunning MJ, Brown GD, Gojis O, Ellis IO, Green AR, et al (2012) Differential oestrogen receptor binding is associated with clinical outcome in breast cancer. Nature **481**: 389–393

Sato Y, Hong SK, Tagiri A, Kitano H, Yamamoto N, Nagato Y, Matsuoka M (1996) A rice homeobox gene, *OSH1*, is expressed before organ differentiation in a specific region during early embryogenesis. Proc Natl Acad Sci USA **93**: 8117–8122

Schuettengruber B, Bourbon HM, Di Croce L, Cavalli G (2017) Genome regulation by Polycomb and Trithorax: 70 years and counting. Cell **171**: 34–57

Serikawa KA, Mandoli DF (1999) *Aaknox1*, a *kn1*-like homeobox gene in *Acetabularia acetabulum*, undergoes developmentally regulated subcellular localization. Plant Mol Biol **41**: 785–793

Shao GN, Lu ZF, Xiong JS, Wang B, Jing YH, Meng XB, Liu GF, Ma HY, Liang Y, Chen F, et al (2019) Tiller bud formation regulators MOC1 and MOC3 cooperatively promote tiller bud outgrowth by activating *FON1* expression in rice. Mol Plant **12**: 1090–1102

Smith HMS, Boschke I, Hake S (2002) Selective interaction of plant homeodomain proteins mediates high DNA-binding affinity. Proc Natl Acad Sci USA **99**: 9579–9584

Smith HMS, Hake S (2003) The interaction of two homeobox genes, *BREVIPEDICELLUS* and *PENNYWISE*, regulates internode patterning in the *Arabidopsis* inflorescence. Plant Cell **15**: 1717–1727

Song S, Chen Y, Liu L, See YHB, Mao C, Gan Y, Yu H (2018) OsFTIP7 determines auxin-mediated anther dehiscence in rice. Nat Plants **4**: 495–504

Sun B, Looi LS, Guo S, He Z, Gan ES, Huang J, Xu Y, Wee WY, Ito T (2014) Timing mechanism dependent on cell division is invoked by Polycomb eviction in plant stem cells. Science **343**: 1248559

Tanaka W, Toriba T, Hirano HY (2017) Three TOB1-related YABBY genes are required to maintain proper function of the spikelet and branch meristems in rice. New Phytol **215**: 825–839

Toriba T, Hirano HY (2014) The *DROOPING LEAF* and *OsETTIN2* genes promote awn development in rice. Plant J **77**: 616–626

Toriba T, Tokunaga H, Shiga T, Nie F, Naramoto S, Honda E, Tanaka K, Taji T, Itoh JI, Kyozuka J (2019) BLADE-ON-PETIOLE genes temporally and developmentally regulate the sheath to blade ratio of rice leaves. Nat Commun **10**:619

Townsley BT, Sinha NR, Kang JL (2013) *KNOX1* genes regulate lignin deposition and composition in monocots and dicots. Front Plant Sci **4**: 121

Trapnell C, Roberts A, Goff L, Pertea G, Kim D, Kelley DR, Pimentel H, Salzberg SL, Rinn JL, Pachter L (2014) Differential gene and transcript expression analysis of RNA-seq experiments with TopHat and Cufflinks. Nat Protoc **9**: 2513–2513

Tsuda K, Ito Y, Sato Y, Kurata N (2011) Positive autoregulation of a KNOX gene is essential for shoot apical meristem maintenance in rice. Plant Cell **23**: 4368–4381

Tsuda K, Kurata N, Ohyanagi H, Hake S (2014) Genome-wide study of KNOX regulatory network reveals brassinosteroid catabolic genes important for shoot meristem function in rice. Plant Cell **26**: 3488–3500

Venglat SP, Dumonceaux T, Rozwadowski K, Parnell L, Babic V, Keller W, Martienssen R, Selvaraj G, Datla R (2002) The homeobox gene *BREVIPEDICELLUS* is a key regulator of inflorescence architecture in *Arabidopsis*. Proc Natl Acad Sci USA **99**: 4730–4735

Wang J, Hu J, Qian Q, Xue HW (2013) LC2 and OsVIL2 promote rice flowering by photoperoid-induced epigenetic silencing of *OsLF*. Mol Plant **6**: 514–527

Wang S, Chang Y, Guo J, Chen JG (2007) *Arabidopsis Ovate Family Protein 1* is a transcriptional repressor that suppresses cell elongation. Plant J **50**: 858–872

Wang W, Lu Y, Li J, Zhang X, Hu F, Zhao Y, Zhou DX (2021) SnRK1 stimulates the histone H3K27me3 demethylase JMJ705 to regulate a transcriptional switch to control energy homeostasis. Plant Cell **33**: 3721–3742

Winter N, Kollwig G, Zhang S, Kragler F (2007) MPB2C, a microtubule-associated protein, regulates non-cell-autonomy of the homeodomain protein KNOTTED1. Plant Cell **19**: 3001–3018

Xiao J, Jin R, Yu X, Shen M, Wagner JD, Pai A, Song C, Zhuang M, Klasfeld S, He C, **et al.** (2017) *Cis* and *trans* determinants of epigenetic silencing by Polycomb repressive complex 2 in *Arabidopsis*. Nat Genet **49**: 1546–1552

Xu L, Shen WH (2008) Polycomb silencing of KNOX genes confines shoot stem cell niches in *Arabidopsis*. Curr Biol **18**: 1966–1971

Yamaguchi T, Nagasawa N, Kawasaki S, Matsuoka M, Nagato Y, Hirano HY (2004) The *YABBY* gene *DROOPING LEAF* regulates carpel specification and midrib development in *Oryza sativa*. Plant Cell **16**: 500–509

Yan WH, Chen DJ, Smaczniak C, Engelhorn J, Liu HY, Yang WJ, Graf A, Carles CC, Zhou DX, Kaufmann K (2018) Dynamic and spatial restriction of Polycomb activity by plant histone demethylases. Nat Plants **4**: 681–689

Yanai O, Shani E, Dolezal K, Tarkowski P, Sablowski R, Sandberg G, Samach A, Ori N (2005) *Arabidopsis* KNOXI proteins activate cytokinin biosynthesis. Curr Biol **15**: 1566–1571

Yang J, Lee S, Hang R, Kim SR, Lee YS, Cao X, Amasino R, An G (2013) OsVIL2 functions with PRC2 to induce flowering by repressing *OsLFL1* in rice. Plant J **73**: 566–578

Yoon J, Cho LH, Antt HW, Koh HJ, An G (2017) KNOX protein OSH15 induces grain shattering by repressing lignin biosynthesis genes. Plant Physiol **174**: 312–325

Yu JR, Lee CH, Oksuz O, Stafford JM, Reinberg D (2019) PRC2 is high maintenance. Genes Dev **33**: 903–935

Yu LF, Patibanda V, Smith HMS (2009) A novel role of BELL1-like homeobox genes, *PENNYWISE* and *POUND-FOOLISH*, in floral patterning. Planta **229**: 693–707

Yuan L, Song X, Zhang L, Yu Y, Liang Z, Lei Y, Ruan J, Tan B, Liu J, Li C (2020) The transcriptional repressors VAL1 and VAL2 recruit PRC2 for genome-wide Polycomb silencing in *Arabidopsis*. Nucleic Acids Res **49**: 98–113

Yuan W, Luo X, Li Z, Yang W, Wang Y, Liu R, Du J, He Y (2016) A *cis* cold memory element and a *trans* epigenome reader mediate Polycomb silencing of *FLC* by vernalization in *Arabidopsis*. Nat Genet **48**: 1527–1534

Zhang LG, Cheng ZJ, Qin RZ, Qiu Y, Wang JL, Cui XK, Gu LF, Zhang X, Guo XP, Wang D, **et al.** (2012) Identification and characterization of an epi-allele of FIE1 reveals a regulatory linkage between two epigenetic marks in rice. Plant Cell **24**: 4407–4421

Zhao Y, Hu Y, Dai M, Huang L, Zhou DX (2009) The WUSCHEL-related homeobox gene *WOX11* is required to activate shoot-borne crown root development in rice. Plant Cell **21**: 736–748

Zheng B, Chen X (2011) Dynamics of histone H3 lysine 27 trimethylation in plant development. Curr Opin Plant Biol **14**: 123–129

Zhou Y, Hartwig B, James GV, Schneeberger K, Turck F (2015) Complementary activities of TELOMERE REPEAT BINDING proteins and Polycomb group complexes in transcriptional regulation of target genes. Plant Cell **28**: 87–101

Zhou Y, Wang Y, Krause K, Yang T, Dongus JA, Zhang Y, Turck F (2018) Telobox motifs recruit CLF/SWN–PRC2 for H3K27me3 deposition via TRB factors in *Arabidopsis*. Nat Genetics **50**: 638–644

Zong W, Tang N, Yang J, Peng L, Ma S, Xu Y, Li G, Xiong L (2016) Feedback regulation of ABA signaling and biosynthesis by a bZIP transcription factor targets drought-resistance-related genes. Plant Physiol **171**: 2810–2825